13

Quantum Injection Dots

Eliade Stefanescu
Center of Advanced Studies in Physics of the Romanian Academy
Romania

1. Introduction

In optoelectronics, quantum dots are essential elements for coupling a device to an electromagnetic field in the infrared domain of the frequency spectrum. Such a dot is a small semiconductor region, with a forbidden band specific to a given application, embedded in the active i-region of the p-i-n junction of a laser structure (1), or in the sensitive i-region of the p-i-n junction of a photovoltaic structure (2). These quantum dots have the advantage of

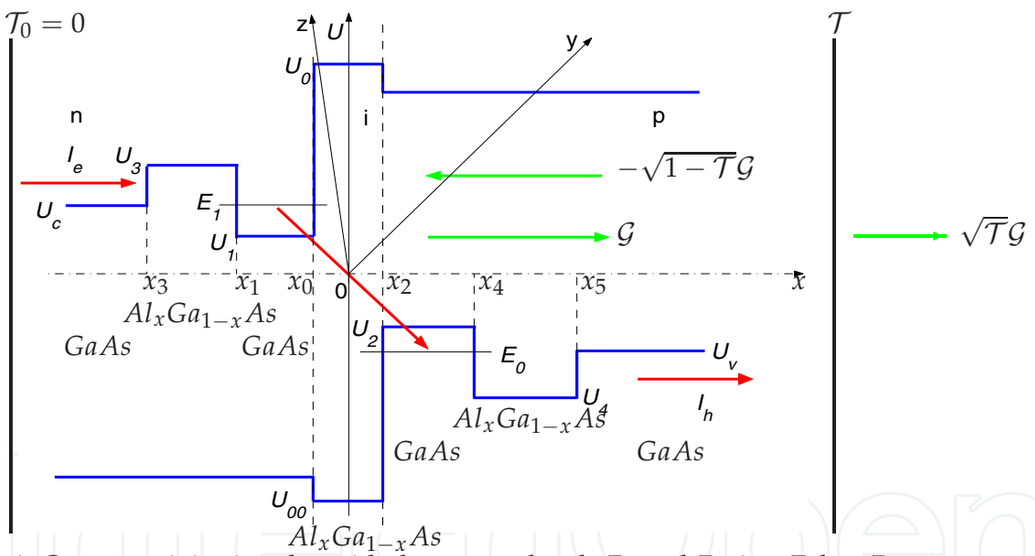

Fig. 1. Quantum injection dot with the energy levels E_1 and E_0, in a Fabry-Perot resonator with transmission coefficients of the mirrors $\mathcal{T}_0 = 0$ and $\mathcal{T} > 0$. By quantum transitions between these levels, a super radiant electromagnetic field with two counter-propagating waves of amplitudes $\mathcal{G}$ and $\sqrt{1-\mathcal{T}}\mathcal{G}$ is generated.

being feasible for a large class of applications (transition frequencies). However, they have the disadvantage that, being embedded in a bulk region, any injection or photovoltaic process includes transport processes through the active (sensitive) region, which are very dissipative. In such a system of quantum dots, an injected electron in the bulk active region of a laser structure has a large probability to recombine with an electron hole before reaching a quantum dot, where this electron becomes an active one, contributing to the laser field generation. Similarly, an optically excited electron in a quantum dot of a photo-voltaic bulk active region, has a large probability to meet another quantum dot, and to decay in the ground state of this

quantum dot before reaching the quasi-neutral zone of the n-region, where this electron brings its contribution to the generated current.

In this chapter, we deal with a different kind of quantum dots (figure 1), as basic elements of a new class of power optoelectronic devices, devoted to the conversion of the environmental heat into usable energy (3–6). Such a quantum dot is substantially different from a bulk quantum dot (1; 2). These dots are deployed in double arrays of donor-acceptor pairs of impurity atoms placed in quantum wells at the two sides of the i-region of an n-i-p junction. The quantum dot density has an appropriate value to include the whole internal field of the semiconductor junction in the quantum dot region, i.e. between the two impurity arrays forming this region. Otherwise, spatial or mobile charge layers arise at the external sides of the two quantum wells, altering the distance $E_1 - E_0$ between the two ground energy levels of these wells. Thus, in a process of current injection, or of an optical current generation, the electrons traverse the internal field region by quantum transitions between the two levels of interest (see figure 1).

In section 2, we derive explicit expressions for electric potentials, energy levels in these potentials, wave-functions, the quantum dot density, and transition dipole moments, which determine the strength of the coupling of a quantum dot to a quasi-resonant electromagnetic field, and to the dissipative environment. We obtain operation conditions for the characteristics of the separation barriers.

In section 3, we consider the dissipative couplings of a quantum injection dot. We describe the dissipative dynamics of such a quantum dot by a master equation for a system of Fermions, coupled to a complex environment of other Fermions, Bosons, and the free electromagnetic field (7). This equation depends on analytic dissipative coefficients, describing correlated transitions of the system particles with the environmental particles, transitions stimulated by thermal fluctuations of the self-consistent field of the environmental Fermions, and the non-Markovian dynamics induced by these fluctuations. We derive explicit expressions of the dissipation coefficients as functions of universal constants and physical properties of the semiconductor structure: effective masses of electrons and electron holes, concentrations of donors and acceptors in the conduction regions, transition frequency, dipole moments, crystal density, elasticity coefficient, geometrical characteristics of the semiconductor structure, and temperature.

In section 4, we consider the dissipative dynamics of an electromagnetic field interacting with the quasi-free electrons of a semiconductor structure. By a method previously used in (7), we obtain a master equation with coefficients depending on frequency and the effective masses, transition dipole moments, and densities of states of these electrons. We derive field equations coupled to the polarizations of the system of active Fermions, with explicit expressions of the coupling and absorption coefficients, as functions of the physical properties of the active quantum dot system, and characteristics of the dissipative environment.

In section 5, we derive equations for the density matrix elements of a quantum injection dot interacting with a quasi-resonant electromagnetic field. We obtain equations for the amplitude mean-values of the forward and backward electromagnetic waves, propagating in a Fabry-Perot cavity which includes a system of such quantum dots. We derive optical equations for a system of quantum injection dots in a resonant Fabry-Perot cavity, with an additional term in the population equation, for describing a current injection in the semiconductor structure (3–5).

In section 6, we present the concept of quantum heat converter, as a device based on systems of quantum injection dots. This device is conceived in two versions: (1) longitudinal quantum heat converter, where the electromagnetic field propagates in the direction of the injected current, i.e. perpendicularly to the semiconductor chip (3; 4), and (2) transversal quantum heat converter, where the electromagnetic field propagates perpendicularly to the injected current, i.e. in the plane of the semiconductor chip (3; 5). Any of these versions could be preferred in specific applications. We derive analytical expressions of the super radiant power, as a function of the injected current, dissipative coefficients, coupling coefficient, number of super radiant transistors, transmission coefficient of the output mirror, and the geometrical characteristics of the device. We get operation conditions for these parameters. We describe the super radiant dissipative dynamics of a quantum injection dot, when a step current is injected in the device.

In this chapter, we present an analytical model depending only on material and geometrical characteristics, temperature, and universal constants.

2. Physical model

The essential problem of any optoelectronic device is the coupling of an electric current to an electromagnetic field. As a function of the roles played by these physical quantities into the input-output characteristic, one can conceive two kinds of devices. In the conventional optoelectronics, a device with the electric current as an input and the electromagnetic field as an output, if this field is not coherent, is called LED. If the output field is coherent, it is called laser. Conversely, if the electric current is the output, depending on an input field, the device is called photodiode, or photovoltaic cell if it is a power device, devoted to the electric energy production.

The new field of the heat conversion optoelectronics, includes two similar kinds of device. In this case, the radiant device is called quantum heat converter (3–5), while the photovoltaic device is called quantum injection system (6). Both kinds of such devices are based on an electron-field interaction with a potential V in the total Hamiltonian

$$H = H_0^S + H^F + V, \tag{1}$$

including a term for an electron with the electric charge $-e$ in an electromagnetic field with the vector potential $\vec{A}$,

$$H_0^S + V = \frac{(\vec{p} + e\vec{A})^2}{2M} + U(\vec{r}), \tag{2}$$

and the Hamiltonian of this field which, for the system represented in figure 1, is of the form

$$H^F = \hbar\omega(a_+^+ a_+ + a_-^+ a_- + 1), \tag{3}$$

where $a_+ - a_+^+$, $a_- - a_-^+$ are the creation-annihilation operators of the two counter-propagating waves. In equation (2), we distinguish the Hamiltonian of the electron in the potential $U(\vec{r})$ of an active quantum dot

$$H_0^S = \frac{\vec{p}^2}{2M} + U(\vec{r}) = \sum_i \varepsilon_i c_i^+ c_i, \tag{4}$$

and the interaction potential

$$V = \frac{e}{M}\vec{p}\vec{A}, \tag{5}$$

while the term in $\vec{A}^2$ is negligible in the non-relativistic approximation. This potential depends on the electron momentum

$$\vec{p} = \mathrm{i}M\sum_{ij}\omega_{ij}\vec{r}_{ij}c_i^+c_j, \tag{6}$$

and the vector potential

$$\vec{A} = \frac{\hbar}{e}\vec{K}\left(a_+e^{\mathrm{i}kx} + a_+^+e^{-\mathrm{i}kx} + a_-e^{-\mathrm{i}kx} + a_-^+e^{\mathrm{i}kx}\right), \tag{7}$$

of the electric field

$$\vec{E} = \mathrm{i}\frac{\hbar\omega}{e}\vec{K}\left(a_+e^{\mathrm{i}kx} - a_+^+e^{-\mathrm{i}kx} + a_-e^{-\mathrm{i}kx} - a_-^+e^{\mathrm{i}kx}\right). \tag{8}$$

In these expressions, M is the electron mass, $c_i^+ - c_j$ are Fermion operators, ω_{ij} are transition frequencies of the active electron, $\vec{r}_{ij}$ are dipole moments, ω is the frequency of the field, and

$$\vec{K} = \vec{1}_y\sqrt{\alpha\frac{\lambda}{\mathcal{V}}} \tag{9}$$

is a vector in the y-direction of this field, depending on the wavelength λ, the fine structure constant $\alpha = \frac{e^2}{4\pi\varepsilon_0\hbar c} \approx \frac{1}{137}$, and the quantization volume $\mathcal{V}$.

From (5) and (6), we notice that the electron-field interaction of the system depends on the transition dipole moment

$$\vec{r}_{01} = \vec{r}_{10} = \int_{\mathcal{V}_s}\Psi_0\vec{r}\Psi_1 d^3\vec{r}, \tag{10}$$

where

$$\Psi_1(x,y,z) = \psi_1(x)\phi_1(y)\chi_1(z) \tag{11a}$$

$$\Psi_0(x,y,z) = \psi_0(x)\phi_0(y)\chi_0(z) \tag{11b}$$

are eigenfunctions of the Hamiltonian (4), for the ground states of the two quantum wells. For the potential $U(\vec{r})$, we distinguish seven regions, of four $GaAs$ quantum wells, and three $Al_xGa_{1-x}As$ potential barriers, determined by the impurity concentrations of these regions (see figure 1). For the two thick conduction regions with the potentials U_c and U_v, we use a three-dimensional model, with a quantization volume $\mathcal{V}_n = 1/N_D$ for the n-region of donor concentration N_D, and $\mathcal{V}_p = 1/N_A$ for the p-region of acceptor concentration N_A. In these quantization volumes, for an electron with the effective mass M_n, and an electron hole with the effective mass M_p, we consider the densities of states (8)

$$g^{(n)}(E_\alpha) = \mathcal{V}_n\frac{\sqrt{2}M_n^{3/2}}{\pi^2\hbar^3}\sqrt{E_\alpha} \tag{12a}$$

$$g^{(p)}(E_\alpha) = \mathcal{V}_p\frac{\sqrt{2}M_p^{3/2}}{\pi^2\hbar^3}\sqrt{E_\alpha}, \tag{12b}$$

and the occupation probabilities of these states with the kinetic energies E_α:

$$f^{(n)}(E_\alpha) = \frac{1}{e^{(U_c+E_\alpha)/T}+1} \approx e^{-(U_c+E_\alpha)/T} \tag{13a}$$

$$f^{(p)}(E_\alpha) = \frac{1}{e^{(-U_v+E_\alpha)/T}+1} \approx e^{-(-U_v+E_\alpha)/T}, \tag{13b}$$

where approximate expressions are taken into account for the usual case of a non-degenerate semiconductor. Considering the integral of the number of particles occupying the states of a quantization volume, one gets the two potentials

$$U_c(T) = T\ln\frac{N_c(T)}{N_D}, \qquad N_c(T) = 2\left(\frac{\sqrt{M_n T/2\pi}}{\hbar}\right)^3 \tag{14a}$$

$$U_v(T) = -T\ln\frac{N_v(T)}{N_A}, \qquad N_v(T) = 2\left(\frac{\sqrt{M_p T/2\pi}}{\hbar}\right)^3. \tag{14b}$$

For the very thin layers of the quantum wells and potential barriers, we use a two-dimensional model. For a quantization area A_e, in n and p regions, one gets the densities of states

$$g^{(1)} = \mathcal{A}_e\frac{M_n}{\pi\hbar^2} \tag{15a}$$

$$g^{(2)} = \mathcal{A}_e\frac{M_p}{\pi\hbar^2}. \tag{15b}$$

By using the Fermi-Dirac distribution in the particle number integral, we obtain expressions similar to (14) for the potentials of the two $GaAs$ quantum wells, as a function of the surface quantum dot density N_e

$$U_1(T) = -T\ln\left(e^{\frac{\pi\hbar^2 N_e}{M_n T}}-1\right) \tag{16a}$$

$$U_2(T) = T\ln\left(e^{\frac{\pi\hbar^2 N_e}{M_p T}}-1\right). \tag{16b}$$

Similar expressions are obtained for the separation barriers, as functions of the donor and acceptor arrays with concentrations N_3, N_4 embedded in the very thin $Al_xGa_{1-x}As$-layers of these barriers,

$$U_3(T) = -T\ln\left(e^{\frac{\pi\hbar^2 N_3}{M_n T}}-1\right) \tag{17a}$$

$$U_4(T) = T\ln\left(e^{\frac{\pi\hbar^2 N_4}{M_p T}}-1\right), \tag{17b}$$

and for the potential barrier U_0 between the two quantum wells,

$$U_0(T) = -T\ln\left(e^{\frac{\pi\hbar^2 N_0}{M_n T}}-1\right), \tag{18}$$

with a slight donor concentration N_0, controlling this potential. For these wells, we consider harmonic wave-functions with exponential tails in the neighboring barriers

$$\psi_1(x) = A_1 \cos\left[k_1(x_0 - x) - \arctan\frac{\alpha_1}{k_1}\right], \quad x_1 \le x \le x_0 \tag{19a}$$

$$\psi_1(x) = A_1\sqrt{\frac{E_1 - U_1}{U_0 - U_1}}e^{-\alpha_1(x-x_0)}, \quad x_0 \le x \le x_2 \tag{19b}$$

$$\psi_1(x) = A_1\sqrt{\frac{E_1 - U_1}{U_3 - U_1}}e^{-\alpha_3(x_1-x)}, \quad x_3 \le x \le x_1 \tag{19c}$$

and

$$\psi_0(x) = A_0 \cos\left[k_0(x - x_2) - \arctan\frac{\alpha_0}{k_0}\right], \quad x_2 \le x \le x_4 \tag{20a}$$

$$\psi_0(x) = A_0\sqrt{\frac{U_2 - E_0}{U_2 - U_{00}}}e^{-\alpha_0(x_2-x)}, \quad x_0 \le x \le x_2 \tag{20b}$$

$$\psi_0(x) = A_0\sqrt{\frac{U_2 - E_0}{U_2 - U_4}}e^{-\alpha_4(x-x_4)}, \quad x_4 \le x \le x_5, \tag{20c}$$

while the tails beyond these barriers are neglected. These wave-functions depend on the wave-numbers

$$k_1 = \frac{1}{\hbar}\sqrt{2M_n(E_1 - U_1)} \tag{21a}$$

$$k_0 = \frac{1}{\hbar}\sqrt{2M_p(U_2 - E_0)}, \tag{21b}$$

attenuation coefficients

$$\alpha_1 = \frac{1}{\hbar}\sqrt{2M_n(U_0 - E_1)} \tag{22a}$$

$$\alpha_0 = \frac{1}{\hbar}\sqrt{2M_p(E_0 - U_{00})} \tag{22b}$$

$$\alpha_3 = \frac{1}{\hbar}\sqrt{2M_n(U_3 - E_1)} \tag{22c}$$

$$\alpha_4 = \frac{1}{\hbar}\sqrt{2M_p(E_0 - U_4)}, \tag{22d}$$

and normalization coefficients

$$A_1 = \sqrt{2}\left[x_0 - x_1 + \frac{\hbar}{\sqrt{2M_n}}\left(\frac{1}{\sqrt{U_0 - E_1}} + \frac{1}{\sqrt{U_3 - E_1}}\right)\right]^{-1/2} \tag{23a}$$

$$A_0 = \sqrt{2}\left[x_4 - x_2 + \frac{\hbar}{\sqrt{2M_p}}\left(\frac{1}{\sqrt{E_0 - U_{00}}} + \frac{1}{\sqrt{E_0 - U_4}}\right)\right]^{-1/2}, \tag{23b}$$

while the energy eigenvalues are given by the equations:

$$E_1 - U_1 = \frac{\hbar^2}{2M_n(x_0 - x_1)^2}\left(\arctan\sqrt{\frac{U_0 - E_1}{E_1 - U_1}} + \arctan\sqrt{\frac{U_3 - E_1}{E_1 - U_1}}\right)^2 \tag{24a}$$

$$U_2 - E_0 = \frac{\hbar^2}{2M_p(x_4 - x_2)^2}\left(\arctan\sqrt{\frac{E_0 - U_{00}}{U_2 - E_0}} + \arctan\sqrt{\frac{E_0 - U_4}{U_2 - E_0}}\right)^2. \tag{24b}$$

We take the two energy eigenvalues as $E_1 = U_c$, $E_0 = U_v$. In this case, the whole internal potential of the n-i-p junction is included on the distance d between the two charge layers of the quantum dot region, which means a quantum dot surface density

$$N_e = \varepsilon\frac{E_1 - E_0}{e^2 d}, \tag{25}$$

while this distance can be approximated as

$$d = \frac{1}{2}(x_2 - x_0 + x_4 - x_1). \tag{26}$$

The energy levels $E_1 = U_c$ and $E_0 = U_v$ can be obtained from (14), as functions of the donor and acceptor concentrations N_D and N_A of the conduction regions. By choosing appropriate values for the separation and quantum dot barriers, from (17) and (18) one gets the surface concentrations N_3, N_4 and N_0 of these barriers. With the widths $x_1 - x_3$ and $x_5 - x_4$, the separation barrier must have a higher penetrability P than the necessary value to provide the injected current I through the device area A_D, which means that the density of this current must be smaller than the thermal current $\frac{1}{6}eN_D v_T P$ emergent from a unit volume with the thermal velocity $v_T = \sqrt{T/M_n}$, and crossing the barrier. We get the conditions

$$\alpha_3(x_1 - x_3) < \frac{1}{2}\ln\left(\frac{eN_D A_D}{6I}\sqrt{\frac{T}{M_n}}\right) \tag{27a}$$

$$\alpha_4(x_5 - x_4) < \frac{1}{2}\ln\left(\frac{eN_A A_D}{6I}\sqrt{\frac{T}{M_p}}\right). \tag{27b}$$

Thus, a quantum injection dot is a two-level system, with the energy levels E_0 and E_1, in a quantization volume shaped as a parallelepiped with the basis area $\mathcal{A} = \frac{1}{N_e}$ and the height $x_5 - x_3$. In this volume, we consider the two wave-functions (19)-(20) for the coordinate x, while, for the coordinates y and z in the plane of the quantum dot array, we consider the wave-functions $\phi_1(y)$, $\phi_0(y)$ and $\chi_1(y)$, $\chi_0(y)$, describing a thermal motion with an energy mean-value T. For a longitudinal device, when the electromagnetic field propagates in the direction x of the injected current, the electric component E_y of this field is coupled with the component y_{01} of the transition dipole moment of the system between thermal states. For a transversal device, when the electromagnetic field propagates in a direction y perpendicular to the direction x of the injected current, i.e. in the plane of the quantum dot array, the electric component E_x of this field is coupled with the transition dipole moment x_{01} between the two states (19)-(20) of the system. These dipole moments also determine the dissipative couplings of the quantum dot. They essentially depend on the width $x_2 - x_0$ of the quantum dot barrier

of height U_0, which determines the overlap of the two wave-functions $\psi_1(x)$ and $\psi_0(x)$. When this width is chosen for reasonable values of the electron-field and dissipative couplings, and N_3, N_4 for reasonable values of the separation barriers satisfying the conditions (27), from equations (16) and (24)-(26) the geometrical characteristics $x_0 x_1, x_2, x_3, x_4$ are obtained.

As an example, for a concentration $N_D = N_A = 3.16 \times 10^{16}\ cm^{-3}$ of a super radiant junction, working at temperature $T = 10\ ^0C$, we get a transition frequency $E_1 - E_0 = 0.1866\ eV$. A quantum dot $Al_{0.37}Ga_{0.63}As$-barrier of $U_0 = 0.5\ eV$ is obtained for a surface concentration of $N_0 = 6.4243 \times 10^6\ m^{-2}$ donors, and separation barriers of $U_3 - U_c = U_v - U_4 = 0.05\ eV$ are obtained for the surface concentrations of these barriers $N_3 = 8.01 \times 10^{13}\ m^{-2}$ and $N_4 = 2.552 \times 10^{13}\ m^{-2}$. For a width $x_2 - x_0 = 5.5\ nm$ of the quantum dot barrier, we get a quantum dot surface concentration $N_e = 1.476 \times 10^{16}\ m^{-2}$ and the widths of the two quantum dot wells $x_0 - x_1 = 4.189\ nm$ and $x_4 - x_2 = 1.576\ nm$, while separation barriers with widths $x_1 - x_3 = 10\ nm$ and $x_5 - x_4 = 3\ nm$ satisfy the conditions (27) for an injected current $I = 45\ A$ in a device with an area $A_D = 4\ cm^2$.

3. Dissipative dynamics of quantum injection dots

We consider a quantum injection dot with two energy levels E_1, E_0, coupled to a super radiant field and a complex dissipative environment of a semiconductor structure as it is represented in figure 1: (1) the quasi-free electrons of the n-conduction region $x < x_3$, (2) the quasi-free holes of the p-conduction region $x > x_5$, (3) the phonons of the crystal at temperature T, and (4) the photons of the free electromagnetic field existing at temperature T (see figure 2). In (3)

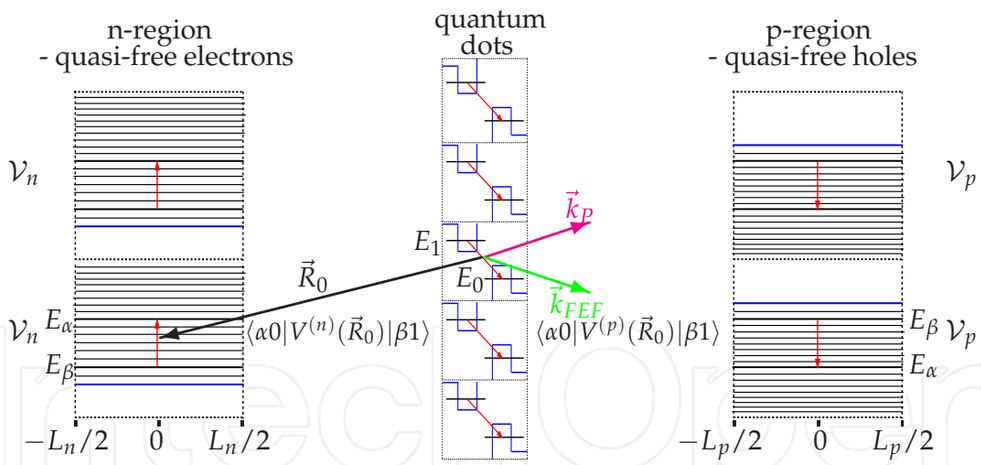

Fig. 2. Dissipative couplings of a quantum injection dot to the environment. A decay $|1\rangle \to |0\rangle$ of the active electron is correlated with: (1) a transition $|\beta\rangle \to |\alpha\rangle$ of a quasi-free electron in a quantization volume $\mathcal{V}_n$, (2) a transition $|\beta\rangle \to |\alpha\rangle$ of a quasi-free hole in a quantization volume $\mathcal{V}_p$, (3) a phonon creation with a wave vector $\vec{k}_P$, and (4) a photon creation with a wave vector $\vec{k}_{FEF}$.

we showed that, for a semiconductor structure with the characteristics mentioned at the end of the preceding section, the decay rate corresponding to the phonon environment is dominant, the decay rate due to the conduction electrons and holes is smaller, while the decay rate given by the free electromagnetic field is negligible.

We consider a system of interest, including a system of Fermions S with the Hamiltonian H_0^S and an electromagnetic field F with the Hamiltonian H^F, in a dissipative environment with the Hamiltonian H^E. Taking into account a potential of interaction V between the Fermion system S and the field F, and a system-environment potential V^E, the dynamics of the total system is described by an equation of motion of the form:

$$\frac{d}{dt}\tilde{\chi}(t) = -\frac{i}{\hbar}\left[\varepsilon\tilde{V}(t) + \varepsilon\tilde{V}^E(t), \tilde{\chi}(t)\right]. \tag{28}$$

In this equation, tilde denotes operators in the interaction picture, e.g.

$$\tilde{\chi}(t) = e^{\frac{i}{\hbar}(H^E+H_0^S+H^F)t}\chi(t)e^{-\frac{i}{\hbar}(H^F+H_0^S+H^E)t}. \tag{29}$$

According to a general procedure disclosed in (9), we take a total density of the form

$$\tilde{\chi}(t) = R\otimes\tilde{\rho}(t) + \varepsilon\tilde{\chi}^{(1)}(t) + \varepsilon^2\tilde{\chi}^{(2)}(t) + ... \ , \tag{30}$$

where $\rho(t)$ is the reduced density matrix of the system of interest, while R is the density matrix of the dissipative environment at the initial moment of time, $t = 0$, the time-evolution of the environment being described by the higher-order terms $\tilde{\chi}^{(1)}(t), \tilde{\chi}^{(2)}(t), ...$ The parameter ε is introduced to handle the orders of the terms in this series expansion, and is set to 1 in the final results. The reduced density of the system is

$$\tilde{\rho}(t) = Tr_E\{\tilde{\chi}(t)\}, \tag{31}$$

while the higher-order terms of the total density have the property:

$$Tr_E\{\tilde{\chi}^{(1)}\} = Tr_E\{\tilde{\chi}^{(2)}\} = ... \ = 0. \tag{32}$$

If initially the environment is in the equilibrium state R, the density matrix of the total system is of the form $\chi(0) = R\rho(0)$. We suppose that at time $t = 0$, due to the interaction V of the system of Fermions with the electromagnetic field, or due to a non-equilibrium initial state $\rho(0) \neq \rho_T$, a time-evolution begins, while the reduced density satisfies a quantum dynamical equation of the form

$$\frac{d}{dt}\tilde{\rho}(t) = \varepsilon\tilde{B}^{(1)}(\tilde{\rho}(t), t) + \varepsilon^2\tilde{B}^{(2)}(\tilde{\rho}(t), t) + ... \ . \tag{33}$$

From the dynamic equation (28), with expressions (30)-(33), we obtain the quantum master equation

$$\begin{aligned}\frac{d}{dt}\rho(t) = &-\frac{\mathrm{i}}{\hbar}[H, \rho(t)] - \mathrm{i}\sum_{ij}\zeta_{ij}[c_i^+c_j, \rho(t)] \\ &+ \sum_{ij}\lambda_{ij}([c_i^+c_j\rho(t), c_j^+c_i] + [c_i^+c_j, \rho(t)c_j^+c_i]) \\ &+ \sum_{ijkl}\zeta_{ij}\zeta_{kl}\int_{t-\tau}^{t}[c_i^+c_j, e^{-\mathrm{i}[\phi(t')+\frac{1}{\hbar}H_0^S(t-t')]}[c_k^+c_l, \rho(t')]e^{\mathrm{i}[\phi(t')+\frac{1}{\hbar}H_0^S(t-t')]}]dt',\end{aligned} \tag{34}$$

where the coefficients

$$\zeta_{ij} = \frac{1}{\hbar}\sqrt{\frac{1}{Y^F}\int_{(\alpha)}\langle\alpha i|(V^F)^2|\alpha j\rangle f_\alpha^F(\varepsilon_\alpha)g_\alpha^F(\varepsilon_\alpha)d\varepsilon_\alpha} \tag{35}$$

describe transitions stimulated by the thermal fluctuations of the self-consistent field of the Y^F environmental Fermions in a certain quantization volume - hopping potential (10), $\phi(t')$ is a phase fluctuation operator, while the coefficients

$$\lambda_{ij} = \lambda_{ij}^F + \lambda_{ij}^B + \gamma_{ij} \tag{36}$$

describe correlated transitions of the system Fermions with environment particles, including explicit terms for Fermions, Bosons, and photons of the free electromagnetic field. These terms depend on the dissipative two-body potentials V^F, V^B, the densities of the environment states $g^F(\varepsilon_\alpha), g^B(\varepsilon_\alpha)$, the occupation probabilities of these states $f^F(\varepsilon_\alpha), f^B(\varepsilon_\alpha)$, and temperature T. For a rather low temperature, $T \ll \varepsilon_{ji}, \ j > i$, these terms become

$$\lambda_{ij}^F = \frac{\pi}{\hbar}|\langle \alpha i|V^F|\beta j\rangle|^2[1 - f^F(\varepsilon_{ji})]g^F(\varepsilon_{ji}) \tag{37a}$$

$$\lambda_{ji}^F = \frac{\pi}{\hbar}|\langle \alpha i|V^F|\beta j\rangle|^2 f^F(\varepsilon_{ji})g^F(\varepsilon_{ji}), \tag{37b}$$

for the Fermion environment,

$$\lambda_{ij}^B = \frac{\pi}{\hbar}|\langle \alpha i|V^B|\beta j\rangle|^2[1 + f^B(\varepsilon_{ji})]g_\alpha^B(\varepsilon_{ji}) \tag{38a}$$

$$\lambda_{ji}^B = \frac{\pi}{\hbar}|\langle \alpha i|V^B|\beta j\rangle|^2 f^B(\varepsilon_{ji})g_\alpha^B(\varepsilon_{ji}) \tag{38b}$$

for the Boson environment, and

$$\gamma_{ij} = \frac{2\alpha}{c^2\hbar^3}\left|\vec{r}_{ij}\right|^2 \varepsilon_{ji}^3(1 + \frac{1}{e^{\varepsilon_{ji}/T} - 1}) \tag{39}$$

for the Boson environment of the free electromagnetic field, where $\vec{r}_{ij}$ are the transition dipole moments. The dissipative terms of the master equation (34) with coefficients (36)-(39) describe correlated transitions of the system and the environment particles, with energy conservation, $\varepsilon_{ji} = \varepsilon_{\alpha\beta}$, in agreement with the quantum-mechanical principles and the detailed balance principle (11). The non-Markovian part of this equation takes into account the fluctuations of the self-consistent field of the environment Fermions, with the coefficients (35).

A significant component of the dissipative dynamics comes from the Coulomb interaction of the active electrons, mainly located in the interval (x_3, x_5), with the conduction electrons and holes in the conduction regions $(-\infty, x_3)$ and $(x_5, +\infty)$, respectively (figure 1). We use the notations $\vec{r}$ for the position vector of an active electron, and $\vec{R}_0 + \vec{R}$ for the position vector of a dissipative electron (hole), where $\vec{R}_0$ is the position vector of an arbitrary n (p) cluster, and $\vec{R} = \vec{1}_x X + \vec{1}_y Y + \vec{1}_z Z$ is the position of an electron (hole) in this cluster (figure 3). In this case, the Coulomb potential in a first-order approximation of the two-body term $\vec{R}\vec{r} = Xx + Yy + Zz$ is

$$V^C(\vec{R}, \vec{r}) = \frac{\alpha\hbar c}{|\vec{R}_0 + \vec{R} - \vec{r}|} \approx \frac{\alpha\hbar c}{|\vec{R}_0|}\left(1 + \frac{Xx + Yy + Zz}{\vec{R}_0^2}\right). \tag{40}$$

From this expression, only the second term, bilinear in the coordinates of an active electron and of an electron (hole) of the environment, yields contributions in the two-body transition matrix elements of the decay (excitation) rates (37):

$$V^F(\vec{R}_0, \vec{R}, \vec{r}) \doteq V^{(n)}(\vec{R}_0, \vec{R}, \vec{r}) = -V^{(p)}(\vec{R}_0, \vec{R}, \vec{r}) = \frac{\alpha\hbar c}{|\vec{R}_0|^3}(Xx + Yy + Zz). \tag{41}$$

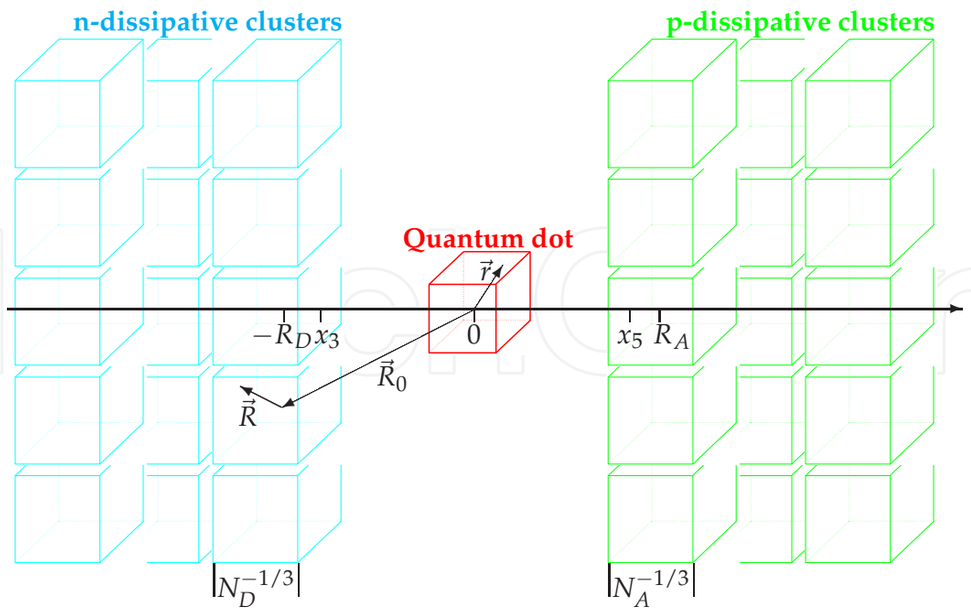

Fig. 3. The electron of a quantum injection dot is coupled to the quasi-free electrons of the n-dissipative clusters (n-region) and quasi-free holes of the p-dissipative clusters (p-region) by an electric dipole-dipole interaction: $V^F(\vec{R}_0, \vec{R}, \vec{r}) = \frac{\alpha\hbar c}{|\vec{R}_0|^3}\vec{R}\vec{r}$.

From the wave-functions derived in the preceding section, we obtain the dipole moment of a quantum dot:

$$x_{01}^{(\Psi)} = c_{01}^{(x)}\left(\frac{x_2 - x_0}{2} - \frac{1}{\alpha_0 - \alpha_1}\right) \tag{42a}$$

$$y_{01}^{(\Psi)} = z_{01}^{(\Psi)} = c_{01}^{(x)}\frac{\hbar}{2\sqrt{M_n T}} \tag{42b}$$

$$y_{10}^{(\Psi)} = z_{10}^{(\Psi)} = c_{01}^{(x)}\frac{\hbar}{2\sqrt{M_p T}}, \tag{42c}$$

as a product of the overlap function

$$c_{01}^{(x)} = \frac{A_1 A_0}{\alpha_0 - \alpha_1}\sqrt{\frac{(E_1 - U_1)(U_2 - E_0)}{(U_0 - U_1)(U_2 - U_{00})}}\left(e^{-\alpha_1(x_2 - x_0)} - e^{-\alpha_0(x_2 - x_0)}\right). \tag{43}$$

and a quantity that we call the state separation distance. At the same time, with the initial and the final energies $E_\beta = T/2,\ E_\alpha = E_\beta + \varepsilon_{10}$, we obtain the dipole moments for the n-zone

$$X_{\alpha\beta}^{(n)} = Y_{\alpha\beta}^{(n)} = Z_{\alpha\beta}^{(n)} = \frac{\hbar}{\varepsilon_{10}}\sqrt{\frac{2\varepsilon_{10} + T}{M_n}} \approx \sqrt{\frac{2\hbar}{M_n\omega_0}}, \tag{44}$$

and for the p-zone,

$$X_{\alpha\beta}^{(p)} = Y_{\alpha\beta}^{(p)} = Z_{\alpha\beta}^{(p)} = \frac{\hbar}{\varepsilon_{10}}\sqrt{\frac{2\varepsilon_{10} + T}{M_p}} \approx \sqrt{\frac{2\hbar}{M_p\omega_0}}, \tag{45}$$

where we used the notations $\varepsilon_{10} \doteq \hbar\omega_0 \doteq E_1 - E_0$. With the quantum dot dipole moments (42), and the environment dipole moments (44)-(45), we calculate the matrix elements of the two-body potential (41). With these matrix elements, from (37) with the densities of states (12) and the occupation probabilities of these states (13), one obtains the dissipative coefficients for the coupling of a quantum dot with a dissipative cluster. By integration over all clusters of both hemispheres of the n and p conduction regions, with the quantization volumes $\mathcal{V}_n = \frac{1}{N_D}$ and $\mathcal{V}_p = \frac{1}{N_A}$ as differential volumes in these integrals, we obtain the dissipation coefficients (3):

$$\lambda_{01}^{(n)} = \frac{4\alpha^2 c^2 \sqrt{2M_n}(\varepsilon_{10} + \frac{T}{2})|c_{01}^{(x)}|^2 \mu_{01}^2}{3\left(\frac{N_D^{-1/3}}{2} - x_3\right)^3 \varepsilon_{10}^{3/2}(e^{-(U_c+\varepsilon_{10})/T} + 1)} \tag{46a}$$

$$\lambda_{10}^{(n)} = \frac{4\alpha^2 c^2 \sqrt{2M_n}(\varepsilon_{10} + \frac{T}{2})|c_{01}^{(x)}|^2 \mu_{01}^2}{3\left(\frac{N_D^{-1/3}}{2} - x_3\right)^3 \varepsilon_{10}^{3/2}(e^{(U_c+\varepsilon_{10})/T} + 1)} \tag{46b}$$

$$\lambda_{01}^{(p)} = \frac{4\alpha^2 c^2 \sqrt{2M_p}(\varepsilon_{10} + \frac{T}{2})|c_{01}^{(x)}|^2 \mu_{01}^2}{3\left(\frac{N_A^{-1/3}}{2} + x_5\right)^3 \varepsilon_{10}^{3/2}(e^{-(-U_v+\varepsilon_{10})/T} + 1)} \tag{46c}$$

$$\lambda_{10}^{(p)} = \frac{4\alpha^2 c^2 \sqrt{2M_p}(\varepsilon_{10} + \frac{T}{2})|c_{01}^{(x)}|^2 \mu_{01}^2}{3\left(\frac{N_A^{-1/3}}{2} + x_5\right)^3 \varepsilon_{10}^{3/2}(e^{(-U_v+\varepsilon_{10})/T} + 1)}, \tag{46d}$$

where

$$\mu_{01}^2 = \left(\frac{x_2 - x_0}{2} - \frac{1}{\alpha_0 - \alpha_1} + \frac{\hbar}{\sqrt{M_n T}}\right)\left(\frac{x_2 - x_0}{2} - \frac{1}{\alpha_0 - \alpha_1} + \frac{\hbar}{\sqrt{M_p T}}\right). \tag{47}$$

is the square of the separation distance of the two states $\Psi_0(\vec{r})$ and $\Psi_1(\vec{r})$. From (35), by similar calculations we obtain the fluctuation coefficients of a quantum dot in the self-consistent field of dissipative clusters:

$$\left[\zeta_{11}^{(n)}\right]^2 = \frac{\alpha^2 c^2 M_n^{3/2} T^{3/2}}{360\pi\sqrt{2\pi}\hbar^3} \cdot \frac{N_D^{1/3}[A_1^2(x_0^3 - x_1^3) + \frac{1}{Ne}]}{N_e N_c \left(\frac{N_D^{-1/3}}{2} - x_3 + \frac{x_0+x_1}{2}\right)^5} \tag{48a}$$

$$\left[\zeta_{11}^{(p)}\right]^2 = \frac{\alpha^2 c^2 M_p^{3/2} T^{3/2}}{360\pi\sqrt{2\pi}\hbar^3} \cdot \frac{N_A^{1/3}[A_1^2(x_0^3 - x_1^3) + \frac{1}{Ne}]}{N_e N_v \left(\frac{N_A^{-1/3}}{2} + x_5 - \frac{x_0+x_1}{2}\right)^5} \tag{48b}$$

$$\left[\zeta_{00}^{(n)}\right]^2 = \frac{\alpha^2 c^2 M_n^{3/2} T^{3/2}}{360\pi\sqrt{2\pi}\hbar^3} \cdot \frac{N_D^{1/3}[A_0^2(x_4^3 - x_2^3) + \frac{1}{Ne}]}{N_e N_c \left(\frac{N_D^{-1/3}}{2} - x_3 + \frac{x_4+x_2}{2}\right)^5} \tag{48c}$$

$$\left[\zeta_{00}^{(p)}\right]^2 = \frac{\alpha^2 c^2 M_p^{3/2} T^{3/2}}{360\pi\sqrt{2\pi}\hbar^3} \cdot \frac{N_A^{1/3}[A_0^2(x_4^3 - x_2^3) + \frac{1}{Ne}]}{N_e N_v \left(\frac{N_A^{-1/3}}{2} + x_5 - \frac{x_4+x_2}{2}\right)^5}. \tag{48d}$$

The Markovian dissipative coefficients (46) describe a very strong, exponential decrease of the decay rate with the width $x_2 - x_0$ of the quantum dot barrier, given by the square of the overlap function (43), and a strong decrease with the distances x_3 and x_5 of the quantum dot separation from the two conduction regions, which enter at the denominators with power 3. The non-Markovian coefficients (48) describe a very strong decrease of the fluctuation rate with the separation distances x_3 and x_5, which enter at the denominators with power 5.

The coupling of a quantum dot electron with a vibrational mode α is described by the potential matrix element (3):

$$V_{01\alpha}^{EP} = V_{10\alpha}^{EP} = -\hbar\omega_0^{3/2} \frac{M\vec{r}_{01}\vec{1}_\alpha}{\sqrt{\mathcal{M}\hbar/2}}, \tag{49}$$

where $\mathcal{M}$ is the mass of the phonon quantization volume $\mathcal{V}_\mathcal{P}$. For the density of phonon states of energy $\hbar\omega_0$, we obtain an expression similar to (12):

$$g_P(\hbar\omega_0) = \mathcal{V}_\mathcal{P} \frac{\sqrt{2}\mathcal{M}^{3/2}}{\pi^2\hbar^3} \sqrt{\hbar\omega_0}. \tag{50}$$

We consider the sound velocity v from the phonon wavelength expressions

$$\lambda_P = \frac{v}{\nu} = \frac{2\pi v}{\omega} = \frac{2\pi\hbar v}{\varepsilon_{10}}, \qquad \lambda_P \equiv \frac{2\pi}{k_P} = \frac{2\pi\hbar}{\sqrt{2\mathcal{M}\varepsilon_{10}}}, \tag{51}$$

and the crystal density

$$D \equiv \frac{\mathcal{M}}{\mathcal{V}_\mathcal{P}} = \frac{2\pi^2\hbar^2}{\mathcal{V}_\mathcal{P}\lambda_P^2\varepsilon_{10}}. \tag{52}$$

With (49)-(52), from (38) we obtain the decay (excitation) rates

$$\lambda_{01}^P = \frac{E_e^2\varepsilon_{10}^5}{\pi\hbar^6c^4v^3D} \cdot \frac{|c_{01}^{(x)}|^2\mu_{01}^2}{1 - e^{-\varepsilon_{10}/T}} \tag{53a}$$

$$\lambda_{10}^P = \frac{E_e^2\varepsilon_{10}^5}{\pi\hbar^6c^4v^3D} \cdot \frac{|c_{01}^{(x)}|^2\mu_{01}^2}{e^{\varepsilon_{10}/T} - 1}, \tag{53b}$$

where $E_e = Mc^2$ is the rest energy of the electron, and v is the sound velocity, which can be calculated from the Young elasticity coefficient E and the crystal density D:

$$v \approx \sqrt{\frac{E}{D}}. \tag{54}$$

We notice that both systems of dissipation coefficients (46) and (53) are proportional to the squares of the state separation distance and overlap function. Expressions (53) describe a very strong dependence of the decay rates on the transition energy ε_{10}, being proportional to this energy with power 5. However, they are valid for phonon wavelengths much larger than the distance between the atoms of the crystal lattice. Otherwise, the number of the density modes can no more be treated as a quasi-continuous function of frequency, and the probability of any non-resonant interaction vanishes (Mösbauer effect). We also found that for the rather low transition energies specific to the quantum injection dots, the decay rate due to the phonon coupling is rather low, e.g. for the structure presented at the end of the preceding section with $\varepsilon_{10} = 0.1866\ eV$, we got $\lambda_{01}^P = 2 \times 10^7\ s^{-1}$. As we found by direct calculations (3), for the quantum injection dots, which are separated by potential barriers from the conduction electrons, the decay rate due to these electrons is much lower than the decay rate due to the coupling to the phonons of the crystal lattice vibrations.

4. Dissipative dynamics of electromagnetic field

The operation of a semiconductor device with quantum dots interacting with a quasi-resonant electromagnetic field is based on the transparency of the host semiconductor structure, with a band to band transition frequency much higher than the quantum dot transition frequency. That means that this electromagnetic field is absorbed by the host semiconductor structure mainly by intra-band transitions, essentially depending on overlap functions of thermal states with excited states populated (depopulated) by these transitions.

The dynamics of this electromagnetic field, with a potential $\tilde{V}(t)$ of interaction with a quantum dot and a potential $\tilde{V}^E(t)$ of interaction with a conduction electron (hole), is described by a system of equations of the form (28), (30), (31) (33), which, in the second-order approximation, provides

$$\frac{d}{dt}\tilde{\rho}(t) = \tilde{B}^{(1)}[\tilde{\rho}(t), t] + \tilde{B}^{(2)}[\tilde{\rho}(t), t] \tag{55a}$$

$$\tilde{B}^{(1)}[\tilde{\rho}(t), t] = -\frac{\mathrm{i}}{\hbar} Tr_E[\tilde{V}(t) + \tilde{V}^E(t), R \otimes \tilde{\rho}(t)] \tag{55b}$$

$$\tilde{\chi}^{(1)}(t) = \int_0^t \left\{ -\frac{\mathrm{i}}{\hbar}[\tilde{V}(t') + \tilde{V}^E(t'), R \otimes \tilde{\rho}(t')] - R \otimes \tilde{B}^{(1)}[\tilde{\rho}(t'), t'] \right\} dt' \tag{55c}$$

$$\tilde{B}^{(2)}[\tilde{\rho}(t), t] = -\frac{\mathrm{i}}{\hbar} Tr_E[\tilde{V}(t) + \tilde{V}^E(t), \tilde{\chi}^{(1)}(t)]. \tag{55d}$$

The interaction potential $\tilde{V}(t)$ is obtained from (5)-(6), while the dissipative potential $\tilde{V}^E(t)$ is given by the similar expressions

$$V^E = \frac{e}{M}\vec{P}\vec{A} \tag{56}$$

and

$$\vec{P} = \mathrm{i}M \sum_{\alpha\beta} \omega_{\alpha\beta} \vec{R}_{\alpha\beta} c_\alpha^+ c_\beta. \tag{57}$$

From (5)-(7) and (56)-(57), we derive expressions of these potentials depending only on the positive transition frequencies $\omega_{ji}(j > i)$ and $\omega_{\alpha\beta}(\alpha > \beta)$, and take into account the so called "rotating-wave approximation", which includes only conservative processes, when an electron excitation is correlated only with a photon annihilation, while an electron decay is correlated only with a photon creation:

$$V = \mathrm{i} \sum_{j>i} \hbar\omega_{ji} \vec{K}\vec{r}_{ij} \left[c_j^+ c_i \left(a_+ e^{\mathrm{i}kx} + a_- e^{-\mathrm{i}kx} \right) - c_i^+ c_j \left(a_+^+ e^{-\mathrm{i}kx} + a_-^+ e^{\mathrm{i}kx} \right) \right] \tag{58}$$

$$V^E = \mathrm{i} \sum_{\alpha>\beta} \hbar\omega_{\alpha\beta} \vec{K}\vec{R}_{\alpha\beta} \left[c_\alpha^+ c_\beta \left(a_+ e^{\mathrm{i}kx} + a_- e^{-\mathrm{i}kx} \right) - c_\beta^+ c_\alpha \left(a_+^+ e^{-\mathrm{i}kx} + a_-^+ e^{\mathrm{i}kx} \right) \right]. \tag{59}$$

We consider the time-dependent expressions of these operators in the interaction picture,

$$\tilde{a}(t) = a e^{-\mathrm{i}\omega t}, \qquad \tilde{a}^+(t) = a^+ e^{\mathrm{i}\omega t} \tag{60}$$

$$\tilde{c}_i^+(t)\tilde{c}_j(t) = c_i^+ c_j e^{-\mathrm{i}\omega_{ji} t}, \qquad \tilde{c}_j^+(t)\tilde{c}_i(t) = c_j^+ c_i e^{\mathrm{i}\omega_{ji} t} \tag{61}$$

$$\tilde{c}_\beta^+(t)\tilde{c}_\alpha(t) = c_\beta^+ c_\alpha e^{-\mathrm{i}\omega_{\alpha\beta} t}, \qquad \tilde{c}_\alpha^+(t)\tilde{c}_\beta(t) = c_\alpha^+ c_\beta e^{\mathrm{i}\omega_{\alpha\beta} t}, \tag{62}$$

and take equations (55) for the mean-values of the electron operators. We retain only the slowly time varying terms, obtained from the resonance condition $\omega_{\alpha\beta} = \omega$, while the rapidly

varying terms are neglected. We consider the summations over the environmental states as integrals over a quasi-continuum of states, with the densities $g(\varepsilon_\alpha)$ and $g(\varepsilon_\beta)$ and occupation probabilities $f(\varepsilon_\alpha)$ and $f(\varepsilon_\beta)$, and neglect the thermal energies $\varepsilon_\beta \sim T$ in comparison with the transition energy $\hbar\omega$. We obtain the quantum master equation

$$\begin{aligned}\frac{d}{dt}\rho(t) = &-\mathrm{i}\omega[a_+^+a_+ + a_-^+a_-,\rho(t)]\\ &+\sum_{j>i}\omega_{ji}\vec{K}\vec{r}_{ij}\left[\langle c_j^+c_i\rangle(a_+e^{\mathrm{i}kx}+a_-e^{-\mathrm{i}kx}) - \langle c_i^+c_j\rangle(a_+^+e^{-\mathrm{i}kx}+a_-^+e^{\mathrm{i}kx}),\rho(t)\right]\\ &+\Lambda\left\{[a_+\rho(t),a_+^+]+[a_+,\rho(t)a_+^+]+[a_-\rho(t),a_-^+]+[a_-,\rho(t)a_-^+]\right\},\end{aligned} \tag{63}$$

with the dissipation coefficient

$$\Lambda = \pi\hbar\omega^2 g(\hbar\omega)(\vec{K}\vec{R}_{\alpha\beta})^2, \tag{64}$$

depending on quantities which, according to (9), (44), and (12), are of the form

$$K = \sqrt{\alpha\frac{\lambda}{\mathcal{V}}} \tag{65}$$

$$R_{\alpha\beta} = \sqrt{\frac{2\hbar}{M\omega}} \tag{66}$$

$$g(\hbar\omega) = \mathcal{V}^S\frac{\sqrt{2}M^{3/2}}{\pi^2\hbar^3}\sqrt{\hbar\omega}. \tag{67}$$

Unlike the master equation for an electromagnetic field mode derived in (12), we considered explicit expressions of the electron-field potential of interaction, and neglected the thermal energy in comparison with the transition energy. With (65)-(67), the dissipation coefficient (64) takes a form

$$\Lambda = \Omega\frac{\mathcal{V}^S}{\mathcal{V}} \tag{68}$$

depending on the quantity

$$\Omega = 4\alpha\sqrt{\frac{2Mc^2\omega}{\hbar}}, \tag{69}$$

and the two quantization volumes, $\mathcal{V}$ of the electromagnetic field and $\mathcal{V}^S$ of the dissipative electron system. We consider a quantization volume $\mathcal{V}^S = V_n = \frac{1}{N_D}$ for an n-type region, or $\mathcal{V}^S = V_p = \frac{1}{N_A}$ for a p-type region. From physical point of view, a quantization volume of the electromagnetic field $\mathcal{V}$ means a measuring process corresponding to a confinement in this volume. The electromagnetic field can not be quantized in a volume $\mathcal{V}^S$, but in a much larger one, with much larger dimensions than the field wavelength λ. For an electromagnetic field, we consider a unit quantization volume $\mathcal{V} = 1_V = 1_L^3 = 1m^3$, because, in this case, the radiation density is equal to the electromagnetic field density times the light velocity, $S = w_E c\ [W/m^2]$, where $w_E = \frac{\varepsilon_0 E^2}{2}\ [J/m^3]$ is calculated with this quantization volume in the expression (8)-(9) of the field.

We notice that the master equation (63) describes an electromagnetic field quantized in a unit volume $\mathcal{V} = 1m^3$ in interaction with an electron system occupying a much smaller volume $\mathcal{V}^S = V^{(n)}$, $V^{(p)}$. A system of N dissipative electrons can be taken into account by multiplying

the dissipative coefficient Λ with N. However, in such a description, the electromagnetic field is considered of a constant amplitude inside the quantization volume $\mathcal{V} = 1_V$, while, in fact, this amplitude undertakes a spatial variation due to the interaction with the system quantized in a volume $\mathcal{V}^S \ll \mathcal{V}$, i.e. propagation characteristics as the absorption coefficient and the refractive index inside the field quantization volume are not taken into account. We take into account the spatial variation of the electromagnetic field by considering this field as being given by an x dependent density matrix, as product of density matrices for the two counter-propagating waves, $\rho(x,t) = \rho_+(x,t)\rho_-(x,t)$, and taking the dissipative terms as integrals over the paths traveled by these waves. Considering a distribution of N_D dissipative clusters over the the thickness L_D of the device, from the master equation (63), we get

$$\frac{d}{dt}\rho_+(x,t) = -\mathrm{i}\omega[a_+^+a_+,\rho_+(x,t)] + \sum_{j>i}\omega_{ji}\vec{K}\vec{r}_{ij}\left[\langle c_j^+c_i\rangle a_+e^{\mathrm{i}kx} - \langle c_i^+c_j\rangle a_+^+e^{-\mathrm{i}kx},\rho_+(x,t)\right] \quad (70a)$$

$$+\frac{\Omega_D}{1_L}\int_0^x \left\{[a_+\rho_+(x',t'),a_+^+] + [a_+,\rho_+(x',t')a_+^+]\right\}e^{-\mathrm{i}k(x-x')}dx'$$

$$\frac{d}{dt}\rho_-(x,t) = -\mathrm{i}\omega[a_-^+a_-,\rho_-(x,t)] + \sum_{j>i}\omega_{ji}\vec{K}\vec{r}_{ij}\left[\langle c_j^+c_i\rangle a_-e^{-\mathrm{i}kx} - \langle c_i^+c_j\rangle (a_-^+e^{\mathrm{i}kx},\rho_-(x,t)\right] \quad (70b)$$

$$+\frac{\Omega_D}{1_L}\int_x^{L_D} \left\{[a_-\rho_-(x',t'),a_-^+] + [a_-,\rho_-(x',t')a_-^+]\right\}e^{-\mathrm{i}k(x'-x)}dx',$$

depending on the dissipative coefficient

$$\Omega_D = \Omega\frac{1_L^2L_D}{1_L^3} = \Omega\frac{L_D}{1_L}, \quad (71)$$

obtained by summation over the dissipative clusters with the volume $1_L^2L_D$ in the quantization volume 1_L^3. The exponential factors in the integrals describe the delay of the field propagating from the coordinate x' of a dissipative element to the coordinate x of the density matrix of this field at this coordinate. These equations describe the dissipative dynamics of a forward electromagnetic wave, propagating from $x' = 0$ to $x' = x$, and of a backward electromagnetic wave, propagating from $x' = L_D$ to $x' = x < L_D$. With these equations, we calculate the mean-values of the field operators

$$a_+(x,t) = \langle a_+\rangle = Tr\left\{a_+\rho_+(x,t)\right\} = \mathcal{A}_+(x,t)e^{-\mathrm{i}\omega t} \quad (72a)$$

$$a_-(x,t) = \langle a_-\rangle = Tr\left\{a_-\rho_-(x,t)\right\} = \mathcal{A}_-(x,t)e^{-\mathrm{i}\omega t}. \quad (72b)$$

For an array of two-level systems with the coordinate x, interacting with the electromagnetic field with the frequency $\omega \approx \omega_0$, we define the time slowly-varying amplitude of the polarization $\mathcal{S}(x,t)$ by the relations

$$\langle c_i^+c_j\rangle = \rho_{ji}(x,t) = \frac{1}{2}\mathcal{S}(x,t)e^{-\mathrm{i}\omega t}, \quad (73)$$

$$\mathcal{S}(x,t) = \mathcal{S}_+(x,t)e^{\mathrm{i}kx} + \mathcal{S}_-(x,t)e^{-\mathrm{i}kx}, \quad (74)$$

where $\mathcal{S}_+(x,t), \mathcal{S}_-(x,t)$ are slowly-varying in space and time amplitudes of the polarization induced by the two counter-propagating waves of the field. Having in view Heisenberg's uncertainty principle

$$\Delta k\Delta x \geq \frac{1}{2}, \qquad \Delta\omega\Delta t \geq \frac{1}{2}, \quad (75)$$

we notice that, in equations (70), this relation selects only the close terms, with $x' \approx x$, while the farer terms in $x - x'$ are washed up by the uncertainty Δk in the oscillating functions under the x'-dependent integrals. By definition, these x-dependent integrals describe the attenuation of an electromagnetic wave squeezed in the x-domain, $\Delta x = 0$. We take into account a finite uncertainty Δx, in the vicinity of x, by extending these x'-integrals with the half-width $\Delta x/2$. We obtain the field equations

$$\frac{d}{dt}\mathcal{A}_+(x,t) = -\frac{1}{2}\omega_0\vec{K}\vec{r}_{01}\mathcal{S}_+(x,t) - \frac{\Omega_D}{1_L}\int_0^{x-\Delta x/2}\mathcal{A}_+(x',t')e^{-\mathrm{i}[k(x-x')-\omega(t-t')]}dx' \quad (76a)$$
$$-\frac{\Omega_D}{1_L}\int_{x-\Delta x/2}^{x+\Delta x/2}\mathcal{A}_+(x',t')e^{-\mathrm{i}[k(x-x')-\omega(t-t')]}dx'$$

$$\frac{d}{dt}\mathcal{A}_-(x,t) = -\frac{1}{2}\omega_0\vec{K}\vec{r}_{01}\mathcal{S}_-(x,t) + \frac{\Omega_D}{1_L}\int_{x+\Delta x/2}^{L_D}\mathcal{A}_-(x',t')e^{-\mathrm{i}[k(x'-x)-\omega(t-t')]}dx' \quad (76b)$$
$$+\frac{\Omega_D}{1_L}\int_{x-\Delta x/2}^{x+\Delta x/2}\mathcal{A}_-(x',t')e^{-\mathrm{i}[k(x'-x)-\omega(t-t')]}dx'.$$

We notice that these are non-local in space equations including retarded contributions of the dissipation processes along the distance $|x - x'|$, and absorption processes in the vicinity Δx of the coordinate x. We consider the quantities under these integrals as spectral lines integrated over half-widths, $k\Delta x - \omega\Delta t = (k + \Delta k)\Delta x - (\omega + \Delta\omega)\Delta t = \Delta k\Delta x - \Delta\omega\Delta t = \frac{\pi}{6} + \frac{\pi}{6} > \frac{1}{2} + \frac{1}{2}$. By integrating the first integral of the first equation two times by parts, for a large distance $x - x'$ we obtain

$$\begin{aligned}\int_0^{x-\Delta x/2}\mathcal{A}_+(x',t')e^{-\mathrm{i}[k(x-x')-\omega(t-t')]}dx' &= \frac{1}{\mathrm{i}k}\,\mathcal{A}_+(x',t')e^{-\mathrm{i}[k(x-x')-\omega(t-t')]}\Big|_0^{x-\Delta x/2}\\ &-\frac{1}{\mathrm{i}k}\int_0^{x-\Delta x/2}\frac{d}{dx'}\mathcal{A}_+(x',t')e^{-\mathrm{i}[k(x-x')-\omega(t-t')]}dx'\\ &= \left[-\frac{\mathrm{i}}{k}\mathcal{A}_+(x,t) + \frac{1}{k^2}\frac{d}{dx}\mathcal{A}_+(x,t)\right]\left[\cos\left(\frac{k\Delta x-\omega\Delta t}{2}\right) - \mathrm{i}\sin\left(\frac{k\Delta x-\omega\Delta t}{2}\right)\right]\\ &= -\frac{1+\mathrm{i}\sqrt{3}}{2k}\mathcal{A}_+(x,t) + \frac{\sqrt{3}-\mathrm{i}}{2k^2}\frac{d}{dx}\mathcal{A}_+(x,t),\end{aligned} \quad (77)$$

while, taking into account that on a vary short distance Δx the field amplitude is practically constant, the second integral of this equation takes a simple form

$$\begin{aligned}\int_{x-\Delta x/2}^{x+\Delta x/2}\mathcal{A}_+(x',t')e^{-\mathrm{i}[k(x-x')-\omega(t-t')]}dx' &= \frac{1}{\mathrm{i}k}\mathcal{A}_+(x',t')e^{-\mathrm{i}[k(x-x')-\omega(t-t')]}\Big|_{x-\Delta x/2}^{x+\Delta x/2}\\ &= \frac{2}{k}\mathcal{A}_+(x,t)\sin\left(\frac{k\Delta x-\omega\Delta t}{2}\right) = \frac{1}{k}\mathcal{A}_+(x,t).\end{aligned} \quad (78)$$

These terms describe a slight variation of the wave-vector k, $k' = k + \kappa$, which means that the amplitude of the mean-value of the field operator takes a form

$$\mathcal{A}_+(x,t) = \tilde{\mathcal{A}}_+(x,t)e^{\mathrm{i}\kappa x}. \quad (79)$$

Taking into account that $\frac{\Omega_D}{ck^2 1_L} \ll 1$, while $\kappa = \frac{k}{1+\frac{2ck^2 1_L}{\sqrt{3}\Omega_D}} \ll k$, we get a field equation

$$\frac{\partial}{\partial t}\mathcal{A}_+(x,t) + c\left[\frac{\partial}{\partial x}\mathcal{A}_+(x,t) + \alpha'\mathcal{A}_+(x,t)\right] = -\frac{1}{2}\omega_0\vec{K}\vec{r}_{01}\mathcal{S}_+(x,t), \quad (80)$$

with an absorption coefficient

$$\alpha' = \frac{2\alpha c}{1_L}\sqrt{\frac{2M}{\hbar\omega}}\frac{L_D}{1_L}. \tag{81}$$

In the following calculations, we are interested in a form of this equation in a cavity with the length L_D,

$$\frac{d}{dt}\mathcal{A}_+(x,t) = -\gamma_F\mathcal{A}_+(x,t) - \frac{1}{2}\omega_0\vec{K}\vec{r}_{01}\mathcal{S}_+(x,t), \tag{82}$$

with a field decay rate

$$\gamma_F = c\alpha' = \frac{2\alpha c^2}{1_L^2}\sqrt{\frac{2M}{\hbar\omega}}L_D, \text{ or } 1_L\gamma_F = \frac{2\alpha c^2}{1_L}\sqrt{\frac{2M}{\hbar\omega}}L_D, \tag{83}$$

which we call field decay velocity. In section 6, it will be shown that the field decay velocity $1_L\gamma_F$ describes the field loss by dissipation, as the quantity $\mathcal{T}c$ describes the electromagnetic energy loss by radiation through the output mirror with the transparency $\mathcal{T}$. We notice that the decay rate of an electromagnetic field in a cavity is proportional to the length of this cavity. For a semiconductor chip with the thickness $L_D = 2\ mm$, we considered in our calculations in (3), from (83) we get a field decay rate $\gamma_F = 2.05 \times 10^7\ s^{-1}$, which is in agreement with the empirical values $\gamma_F = 10^7,\ 10^8\ s^{-1}$, we considered in these calculations. It is interesting that, in this model, the decay rate does not depend on the concentration of the dissipative clusters, since an increase of this concentration means a decrease of the density of states in every cluster, which, in this way, becomes smaller. These two variations cancel exactly one another in the final result. By taking into account the spreading of a dissipative electron wave-function beyond the the boundaries of its cluster due to the thermal motion, one obtains a lower value of the decay rate, but with an increase with the concentration of these clusters.

5. Optical equations for a system of quantum injection dots

From the quantum master equation (34), we derive optical equations for a two-level system. In the approximation of the slowly varying amplitudes, we consider the non-diagonal matrix elements

$$\rho_{10}(t) = \rho_{01}^*(t) = \frac{1}{2}\left[\mathcal{S}_+(t)e^{ikx} + \mathcal{S}_-(t)e^{-ikx}\right]e^{-i\omega t}, \tag{84}$$

and the population difference

$$w(t) = \rho_{11}(t) - \rho_{00}(t), \text{ with the normalization condition} \tag{85a}$$

$$1 = \rho_{11}(t) + \rho_{00}(t). \tag{85b}$$

Calculating the matrix elements of the two-level system, and averaging over the field states, from the master equation (34) we get:

$$\begin{aligned}\frac{d}{dt}\rho_{10}(t) = & -[\lambda_{01} + \lambda_{10} + i(\omega_0 + \zeta_{11} - \zeta_{00})]\rho_{10}(t) \\ & + \vec{K}\left[(\langle a_+\rangle + \langle a_-^+\rangle)e^{ikx} + (\langle a_+^+\rangle + \langle a_-\rangle)e^{-ikx}\right]\omega_0\vec{r}_{10}[\rho_{00}(t) - \rho_{11}(t)] \\ & + (\zeta_{11} - \zeta_{00})^2\int_{t-\tau}^{t}\rho_{10}(t')e^{-i[\phi_{10}(t') + \omega(t-t')]}dt'\end{aligned} \tag{86a}$$

$$\begin{aligned}\frac{d}{dt}\rho_{11}(t) = & -\frac{d}{dt}\rho_{00}(t) = 2[\lambda_{10}\rho_{00} - \lambda_{01}\rho_{11}] \\ & + \vec{K}\left[(\langle a_+\rangle + \langle a_-^+\rangle)e^{ikx} + (\langle a_+^+\rangle + \langle a_-\rangle)e^{-ikx}\right]\omega_0\vec{r}_{10}[\rho_{10}(t) + \rho_{01}(t)].\end{aligned} \tag{86b}$$

From the expression (8) of the quantized electric field $\vec{E}$ in the plane-wave approximation, and mean-values of the annihilation operators of the form

$$\langle a_+ \rangle = \bar{a}_+(t)e^{-\mathrm{i}\omega t} \tag{87a}$$

$$\langle a_- \rangle = \bar{a}_-(t)e^{-\mathrm{i}\omega t}, \tag{87b}$$

we get the mean-value of this field,

$$\langle \vec{E} \rangle = \frac{1}{2}\left[\vec{\mathcal{E}}(t)e^{-\mathrm{i}\omega t} + \vec{\mathcal{E}}^*(t)e^{\mathrm{i}\omega t}\right], \tag{88}$$

with the time slowly-varying amplitude

$$\vec{\mathcal{E}}(t) = \vec{\mathcal{E}}_+(t)e^{\mathrm{i}kx} + \vec{\mathcal{E}}_-(t)e^{-\mathrm{i}kx}, \tag{89}$$

while the amplitudes of the two counter-propagating waves are

$$\vec{\mathcal{E}}_+(t) = 2\mathrm{i}\frac{\hbar\omega}{e}\vec{K}\bar{a}_+(t) \tag{90a}$$

$$\vec{\mathcal{E}}_-(t) = 2\mathrm{i}\frac{\hbar\omega}{e}\vec{K}\bar{a}_-(t). \tag{90b}$$

In this description we neglect the variation of the amplitudes inside the cavity, by taking into account these two amplitudes only as mean-values over the space coordinate, related by the boundary condition for the output mirror of transmission coefficient $\mathcal{T}$:

$$\vec{\mathcal{E}}_-(t) = -\sqrt{1-\mathcal{T}}\,\vec{\mathcal{E}}_+(t). \tag{91}$$

With the notations

$$\vec{g} = \frac{e}{\hbar}\vec{r}_{10} \tag{92}$$

for the coupling coefficient,

$$\gamma_\perp = \lambda_{01} + \lambda_{10} \tag{93}$$

for the dephasing rate,

$$\gamma_\parallel = 2(\lambda_{01} + \lambda_{10}) \tag{94}$$

for the decay rate,

$$\gamma_n = |\zeta_{11} - \zeta_{00}| \tag{95}$$

for the fluctuation rate of the self-consistent field, and

$$w_T = -\frac{\lambda_{01} - \lambda_{10}}{\lambda_{01} + \lambda_{10}}, \tag{96}$$

from (84)-(91) we obtain equations for the slowly-varying amplitudes

$$\begin{aligned}\frac{d}{dt}\mathcal{S}_+(t) = \; & -[\gamma_\perp + \mathrm{i}(\omega_0 + \gamma_n - \omega)]\mathcal{S}_+(t) + \mathrm{i}\vec{g}\vec{\mathcal{E}}_+(t)w(t) \\ & +\gamma_n^2\int_{t-\tau}^{t}\mathcal{S}_+(t')e^{-\mathrm{i}[\phi_{10}(t')+\omega(t-t')]}dt'\end{aligned} \tag{97a}$$

$$\frac{d}{dt}w(t) = -\gamma_\parallel[w(t) - w_T] + (2-\mathcal{T})\mathrm{i}\vec{g}\frac{1}{2}\left[\vec{\mathcal{E}}_+^*(t)\mathcal{S}_+(t) - \vec{\mathcal{E}}_+(t)\mathcal{S}_+^*(t)\right]. \tag{97b}$$

In equation (97b) we have taken into account that the term

$$\Phi_+(t) = \mathrm{i}\vec{g}\frac{1}{2}\left[\vec{\mathcal{E}}_+^*(t)\mathcal{S}_+(t) - \vec{\mathcal{E}}_+(t)\mathcal{S}_+^*(t)\right] \tag{98}$$

is a particle flow due to the forward electromagnetic wave propagating in the cavity, while

$$\Phi_-(t) = \mathrm{i}\vec{g}\frac{1}{2}\left[\vec{\mathcal{E}}_-^*(t)\mathcal{S}_-(t) - \vec{\mathcal{E}}_-(t)\mathcal{S}_-^*(t)\right] \tag{99}$$

is a particle flow due to the backward electromagnetic wave, which means that the two flows satisfy the boundary condition for the energy flow of the electromagnetic field

$$\Phi_-(t) = (1-\mathcal{T})\Phi_+(t). \tag{100}$$

At the same time, calculating the mean-value of the field operator a, averaging over the states of the two-level system, and taking into account the relation

$$\langle c_i^+ c_j\rangle = \rho_{ji}(t), \tag{101}$$

from equation (34) we get the field equation

$$\frac{d}{dt}\langle a_+\rangle = -\mathrm{i}\omega\langle a_+\rangle + \vec{K}\omega_0\vec{r}_{10}[\rho_{10}(t) - \rho_{01}(t)]e^{-\mathrm{i}kx}. \tag{102}$$

Thus, with (84), (87) and (90), we get a field equation for slowly-varying amplitudes

$$\frac{d}{dt}\vec{\mathcal{E}}_+(t) = -\mathrm{i}\omega_0\frac{\hbar\omega}{e}\vec{K}(\vec{K}\vec{r}_{10})\mathcal{S}_+(t). \tag{103}$$

We consider this equation for the components $u(t)$ and $v(t)$ of the polarization amplitude

$$\mathcal{S}_+(t) = u(t) - \mathrm{i}v(t), \tag{104}$$

and $\mathcal{F}(t)$ and $\mathcal{G}(t)$ of the electromagnetic field

$$\mathcal{E}_+(t) = \mathcal{F}(t) + \mathrm{i}\mathcal{G}(t), \tag{105}$$

and take into account the field dissipation described by the dissipation rate γ_F. We get

$$\frac{d}{dt}\mathcal{F}(t) = -\gamma_F\mathcal{F}(t) - g\frac{\hbar\omega_0}{2\varepsilon\mathcal{V}}v(t) \tag{106a}$$

$$\frac{d}{dt}\mathcal{G}(t) = -\gamma_F\mathcal{G}(t) - g\frac{\hbar\omega_0}{2\varepsilon\mathcal{V}}u(t). \tag{106b}$$

We consider these equations for the electromagnetic energy in the quantization volume $\mathcal{V}$, and introduce the energy flow through the surface $\mathcal{A}$ of this volume:

$$\frac{d}{dt}\left[\mathcal{V}\frac{1}{2}\varepsilon\mathcal{F}^2(t)\right] = -\mathcal{T}c\frac{1}{2}\varepsilon\mathcal{F}^2(t)\mathcal{A} - \gamma_F\mathcal{V}\varepsilon\mathcal{F}^2(t) - g\frac{\hbar\omega_0}{2}\mathcal{F}v(t) \tag{107a}$$

$$\frac{d}{dt}\left[\mathcal{V}\frac{1}{2}\varepsilon\mathcal{G}^2(t)\right] = -\mathcal{T}c\frac{1}{2}\varepsilon\mathcal{G}^2(t)\mathcal{A} - \gamma_F\mathcal{V}\varepsilon\mathcal{G}^2(t) - g\frac{\hbar\omega_0}{2}\mathcal{G}u(t). \tag{107b}$$

At the same time, from (97b) with (104) and (105), we derive the equation for the population difference (85a), and introduce the particle flow $\mathcal{I}$ in a two-level system, due to the electric current $I = eA_D N_e \mathcal{I}$ injected in the device:

$$\frac{d}{dt}w(t) = -\gamma_F[w(t) - w_T] + 2\mathcal{I} + (2-\mathcal{T})g[\mathcal{F}(t)v(t) + \mathcal{G}(t)u(t)] \tag{108}$$

From (107) and (108) with (85), we get an equation of energy conservation:

$$\begin{aligned}\hbar\omega_0\mathcal{I} = \frac{d}{dt}\left\{\hbar\omega_0\rho_{11}(t) + (2-\mathcal{T})\mathcal{V}\frac{1}{2}\varepsilon[\mathcal{F}^2(t) + \mathcal{G}^2(t)]\right\} + \gamma_\parallel\left[\rho_{11}(t) - \frac{1+w_T}{2}\right]\hbar\omega_0 \\ +(2-\mathcal{T})(\mathcal{T}c\frac{\mathcal{A}}{\mathcal{V}} + 2\gamma_F)\mathcal{V}\frac{1}{2}\varepsilon[\mathcal{F}^2(t) + \mathcal{G}^2(t)].\end{aligned} \tag{109}$$

This equation describes the transition power $\hbar\omega_0\mathcal{I}$ of the active system providing the energy transfer processes involved in the dissipative super radiant decay: (1) the energy variation of the electron-field system, (2) the dissipative decay of the electron energy, proportional to $\gamma_\parallel$, (3) the radiation of the field energy, proportional to the light velocity c and the transmission coefficient $\mathcal{T}$ of the output mirror, and (4) the dissipation of the field energy, proportional to γ_F. In this equation, both waves leaving the quantum system and propagating in the cavity, the forward wave with an amplitude coefficient 1 and the backward wave with an amplitude coefficient $\mathcal{R} = 1 - \mathcal{T}$, are taken into account with the coefficient $1 + \mathcal{R} = 2 - \mathcal{T}$.

From the polarization equation (97a) with (104) and (105), the population equation (108), and the field equations (107), we obtain the equations of the slowly varying amplitudes of the system:

$$\frac{d}{dt}u(t) = -\gamma_\perp[u(t) - \delta\omega v(t)] - g\mathcal{G}(t)w(t) \tag{110a}$$

$$+\gamma_n^2\int_{t-\tau}^{t}\left\{u(t')\cos[\phi_n(t') + (\omega-\omega_0)(t-t')] + v(t')\sin[\phi_n(t') + (\omega-\omega_0)(t-t')]\right\}dt'$$

$$\frac{d}{dt}v(t) = -\gamma_\perp[v(t) + \delta\omega u(t)] - g\mathcal{F}(t)w(t) \tag{110b}$$

$$+\gamma_n^2\int_{t-\tau}^{t}\left\{v(t')\cos[\phi_n(t') + (\omega-\omega_0)(t-t')] - u(t')\sin[\phi_n(t') + (\omega-\omega_0)(t-t')]\right\}dt'$$

$$\frac{d}{dt}w(t) = -\gamma_\parallel[w(t) - w_T] + 2\mathcal{I} + (2-\mathcal{T})g[\mathcal{G}(t)u(t) + \mathcal{F}(t)v(t)] \tag{110c}$$

$$\frac{d}{dt}\mathcal{F}(t) = -\frac{1}{2}\mathcal{T}c\frac{\mathcal{A}}{\mathcal{V}}\mathcal{F}(t) - \gamma_F\mathcal{F}(t) - g\frac{\hbar\omega_0}{2\varepsilon\mathcal{V}}v(t) \tag{110d}$$

$$\frac{d}{dt}\mathcal{G}(t) = -\frac{1}{2}\mathcal{T}c\frac{\mathcal{A}}{\mathcal{V}}\mathcal{G}(t) - \gamma_F\mathcal{G}(t) - g\frac{\hbar\omega_0}{2\varepsilon\mathcal{V}}u(t), \tag{110e}$$

where $\phi_n(t') \equiv \phi_{01}(t') \equiv -\phi_{10}(t')$ is the phase fluctuation with a fluctuation time $\tau_n = 1/\gamma_n$, and

$$\delta\omega = \frac{\omega - \omega_0 - \gamma_n}{\gamma_\perp} \tag{111}$$

is the relative atomic detuning. In these equations, the coupling of the electron system to the electromagnetic field is described by a coupling coefficient for the dipole interaction $g = \vec{g}\vec{1}_E$. These equations also describe a dissipative decay of the electron system by the coefficients $\gamma_\parallel$

and $\gamma_\perp$, non-Markovian effects by time-integrals proportional to the fluctuation coefficient γ_n^2 in the polarization equations (110a) and (110b), a decrease of the electron-field coupling due to the field radiation by the term proportional to the coefficient $(2-\mathcal{T})$ in (110c), and a decrease of field by the radiation terms proportional to the product $c\mathcal{T}$ in (110d) and (110e), and by the terms proportional to the decay rate γ_F.

6. Superradiant quantum injection dots and heat conversion

The dynamic equations (110) take a simpler form in a stationary regime when the derivatives with time become zero and the polarization variables can be taken out from the integrals. Considering an integration over a fluctuation time $\tau_n = 1/\gamma_n$, we get a time oscillating term, generated by the fluctuations of the environment particles. In the Markovian approximation, when these oscillations are neglected, we get the steady-state equations:

$$-\gamma_\perp[u - \delta\omega v] - g\mathcal{G}w = 0 \tag{112a}$$
$$-\gamma_\perp[v + \delta\omega u] - g\mathcal{F}w = 0 \tag{112b}$$
$$-\gamma_\parallel(w - w_T) + 2\mathcal{I} + (2-\mathcal{T})g(\mathcal{G}u + \mathcal{F}v) = 0 \tag{112c}$$
$$-\Gamma_F\mathcal{F} - Gv = 0 \tag{112d}$$
$$-\Gamma_F\mathcal{G} - Gu = 0, \tag{112e}$$

where

$$G = g\frac{\hbar\omega_0}{2\varepsilon\mathcal{V}} \tag{113a}$$
$$\Gamma_F = \frac{1}{2}\mathcal{T}c\frac{\mathcal{A}}{\mathcal{V}} + \gamma_F. \tag{113b}$$

From the system of equations (112), for the resonance case ($\delta\omega = 0$), we calculate the flow density of the electromagnetic energy radiated by the device:

$$S = \mathcal{T}c\frac{1}{2}\varepsilon(\mathcal{F}^2 + \mathcal{G}^2). \tag{114}$$

We get

$$S = \frac{\frac{\hbar\omega_0}{(2-\mathcal{T})\mathcal{A}}}{1 + \frac{2\gamma_F\mathcal{V}}{\mathcal{T}c\mathcal{A}}}\left[\mathcal{I} - \left(-w_T\frac{\gamma_\parallel}{2} + \frac{\frac{1}{2}\mathcal{T}c\frac{\mathcal{A}}{\mathcal{V}} + \gamma_F}{\frac{g^2\hbar\omega_0}{\gamma_\perp\gamma_\parallel\varepsilon\mathcal{V}}}\right)\right]. \tag{115}$$

This expression of the flow density S has a nice physical interpretation, being proportional to the product of the transition energy $\hbar\omega_0$, divided to the radiation area of a quantum dot $\mathcal{A}$, with the difference between the particle flow $\mathcal{I}$ and a threshold value depending on coupling, radiation, and dissipation coefficients. This expression is valid when the quantization volume $\mathcal{V}$ of the field corresponds to the electromagnetic energy delivered by the whole system of N_eN_t quantum dots to a volume unit, which means

$$\mathcal{V}[m^3] = \frac{1}{N_e[m^{-2}]N_t[m^{-1}]}, \tag{116}$$

where $N_e[m^{-2}]$ is the number of quantum dots per area unit, and $N_t[m^{-1}]$ is the number of super radiant junctions per length unit.

In a first approximation, we neglect the temperature variation due to the heat transfer through the semiconductor structure. To take into account this temperature variation, one has to make corrections of the parameters, to obtain the same transition frequency on the whole chain of super radiant junctions.

Such a device can be realized in two versions schematically represented in figure 4: (a) a longitudinal device, with the two mirrors M_1 and M_2 made on the two surfaces in the plane of the chip, of transmission coefficients $\mathcal{T}_0 = 0$ and $\mathcal{T} > 0$, which form a Fabry-Perot cavity coupling a super radiant mode that propagates in the x-direction of the injection current; (b) a transversal device, with the two mirrors M_1 and M_2 made on two lateral surfaces of the chip, of transmission coefficients $\mathcal{T}_0 = 0$ and $\mathcal{T} > 0$, which form a Fabry-Perot cavity coupling a super radiant mode that propagates in the y-direction, perpendicular to the injection current. While in version (a) the roles of the mirrors M_1 and M_2, and of the injection electrodes $\mathcal{E}_1$ and $\mathcal{E}_2$, are played by the same metalizations, made on the two surfaces in the plane of the chip, in version (b) the mirror metalizations M_1 and M_2, which are made on two lateral surfaces, are different from the electrode metalizations $\mathcal{E}_1$ and $\mathcal{E}_2$.

The two devices have the same structure, including layers of $GaAs$, with a narrower forbidden band and a heavier doping, for the quantum wells, and layers of $Al_xGa_{1-x}As$, with a larger forbidden band and a lighter doping, for the potential barriers. The margins of these bands are determined by the concentrations of the donors (acceptors) embedded in the semiconductor layers. For a longitudinal device (figure 4a), the $\bar{N}_t$ (dimensionless) quantum dots in the x-direction, radiate through an area $\dfrac{1}{N_e[m^{-2}]}$, which means

$$\mathcal{A}_L[m^2] = \frac{1}{N_e[m^{-2}]\bar{N}_t}, \tag{117}$$

while for a transversal device (see figure 4b), the $\sqrt{N_e[m^{-2}]A_D[m^2]}$ quantum dots in the y-direction, radiate through an area $\dfrac{L_D[m]}{\bar{N}_t}\dfrac{1}{\sqrt{N_e[m^{-2}]}}$, which means

$$\mathcal{A}_T[m^2] = \frac{L_D[m]}{N_e[m^{-2}]\bar{N}_t\sqrt{A_D[m^2]}}. \tag{118}$$

With the radiation area $\mathcal{A}_L$ ($\mathcal{A}_T$) of a quantum dot, from (115) we derive the flow density S_L (S_D), and the total flow of the electromagnetic field radiated by the device in the two versions:

$$\Phi_L = A_D S_L \tag{119a}$$

$$\Phi_T = L_D\sqrt{A_D}S_T. \tag{119b}$$

We obtain

$$\Phi_L = \frac{\bar{N}_t}{(2-\mathcal{T})\left(1+2\frac{1_L\gamma_F}{\mathcal{T}c}\right)}\cdot\frac{\hbar\omega_0}{e}(I-I_{0L}) \tag{120a}$$

$$\Phi_T = \frac{\bar{N}_t}{(2-\mathcal{T})\left(1+2\frac{1_L\gamma_F}{\mathcal{T}c}\frac{A_D^{1/2}}{L_D}\right)}\cdot\frac{\hbar\omega_0}{e}(I-I_{0T}), \tag{120b}$$

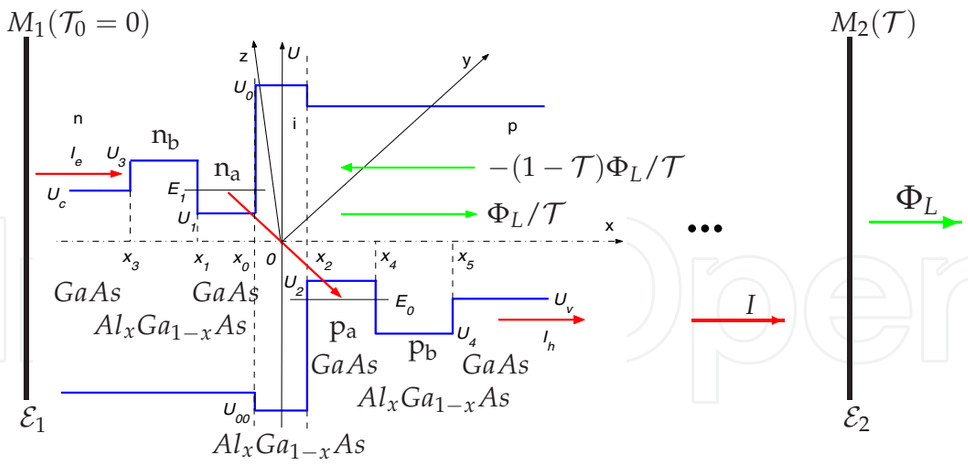

(a) Longitudinal super radiant device with the Fabry-Perot cavity oriented in the x-direction of the injected current $I = I_e = I_h$, i.e. perpendicular to the semiconductor layers.

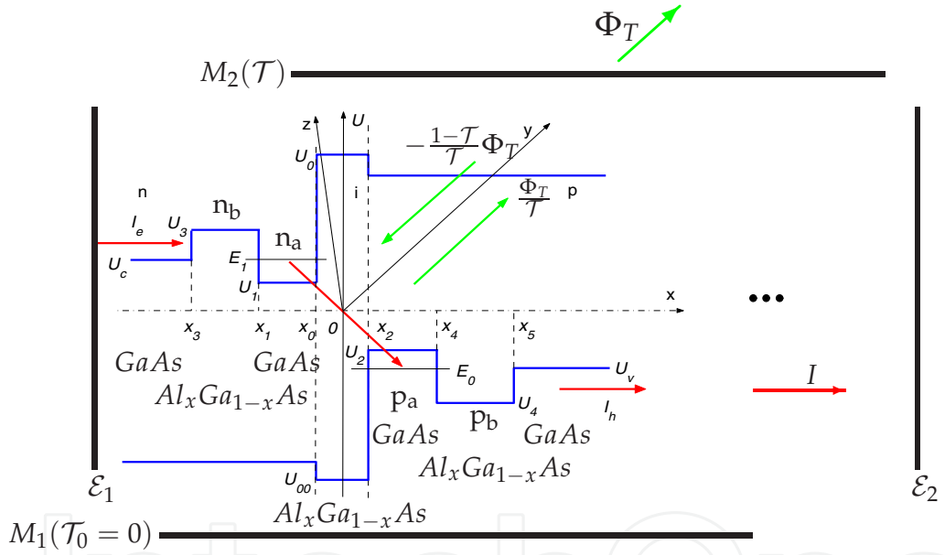

(b) Transversal super radiant device with the Fabry-Perot cavity oriented in the y-direction, perpendicular to the injected current $I = I_e = I_h$, i.e. in the plane of the semiconductor layers.

Fig. 4. Dissipative super radiant n-i-p device with two injection electrodes $\mathcal{E}_1$ and $\mathcal{E}_2$ and a Fabry-Perot cavity with the mirrors M_1 and M_2 of transmission coefficients $\mathcal{T}_0 = 0$ and $\mathcal{T}$, respectively, in two possible versions (a) and (b).

as a function of the injected current I and the threshold currents

$$I_{0L} = \frac{1}{2} e N_e A_D \gamma_{\parallel} \left[-w_T + \frac{\varepsilon \gamma_{\perp}}{g_L^2 \hbar \omega_0 N_e \bar{N}_t} (\mathcal{T} c + 2 \cdot 1_L \gamma_F) \right] \tag{121a}$$

$$I_{0T} = \frac{1}{2} e N_e A_D \gamma_{\parallel} \left[-w_T + \frac{\varepsilon \gamma_{\perp}}{g_T^2 \hbar \omega_0 N_e \bar{N}_t} (\mathcal{T} c \frac{L_D}{A_D^{1/2}} + 2 \cdot 1_L \gamma_F) \right], \tag{121b}$$

which depends on the field decay velocity (83). The threshold current is proportional to the threshold population, which includes three terms for the three dissipative processes that must be balanced by current injection for creating a coherent electromagnetic field: (1) a term $-w_T$, for a population inversion, (2) a term proportional to the light velocity c and the transmission coefficient $\mathcal{T}$, for the field radiation, and (3) a term proportional to decay rate γ_F, for the field dissipation.

From (112c) and (120), we notice that when the injection current $I = eN_eA_D\mathcal{I}$ is under the threshold value I_{0L} (I_{0T}), the radiation field is $\mathcal{F} + i\mathcal{G} = 0$, while the population difference w increases with this current. When the injection current I reaches the threshold current I_{0L} (I_{0T}), the population difference w reaches the radiation value

$$w_R = \frac{\mathcal{T}c\frac{\mathcal{A}}{\mathcal{V}} + 2\gamma_F}{\frac{g^2\hbar\omega_0}{\gamma_\perp\varepsilon\mathcal{V}}}. \tag{122}$$

Increasing the injection current I beyond the threshold value I_{0L} (I_{0T}), the population difference keeps this value, while the super radiant field and the polarization ($u = -\frac{g}{\gamma_\perp}w_R\mathcal{G}, v = -\frac{g}{\gamma_\perp}w_R\mathcal{F}$) increases. However, the polarization (u, v) can not increase indefinitely, being constrained by the condition of the Bloch vector length $(2-\mathcal{T})(u^2 + v^2) + w^2 \leq w_T^2$. For the maximum value (u_M, v_M) of the polarization, while $u_M^2 + v_M^2 = (w_T^2 - w_R^2)/(2-\mathcal{T})$, the super radiant field reaches its maximum flow density

$$S_M = \frac{\mathcal{T}c\varepsilon}{2(2-\mathcal{T})}\left[w_T^2\frac{g^2\frac{\hbar^2\omega_0^2}{\varepsilon^2\mathcal{V}^2}}{\left(\mathcal{T}c\frac{\mathcal{A}}{\mathcal{V}} + 2\gamma_F\right)^2} - \frac{\gamma_\perp^2}{g^2}\right]. \tag{123}$$

From this equation with equation (115) for $S = S_M$, we get the value $I_M = eN_eA_D\mathcal{I}_M$ of the injection current producing the maximum flow of the electromagnetic energy. Increasing the injection current beyond this value, the polarization (u, v) will not increase any more, but the population will increase, leading to a rapid decrease of the polarization. Neglecting the current increase from I_M to the value I'_M when the polarization vanishes, from equation (112c) with $w = -w_T$ and $u = v = 0$, we get a simple, approximate expression $I_M \approx I'_M = \frac{1}{2}eN_eA_D\gamma_\parallel(-w_T - w_T)$, which can be compared with (121). From the operation condition $I_{0L}, I_{0T} < I_M$, we get conditions for the coupling, dissipation, and radiation coefficients:

$$w_{IL} = \frac{\varepsilon_0\gamma_\perp}{g_L^2\hbar\omega_0N_e\bar{N}_t}(\mathcal{T}c + 21_L\gamma_F) < -w_T \approx 1 \tag{124a}$$

$$w_{IT} = \frac{\varepsilon_0\gamma_\perp}{g_T^2\hbar\omega_0N_e\bar{N}_t}(\mathcal{T}c\frac{L_D}{A_D^{1/2}} + 21_L\gamma_F) < -w_T \approx 1. \tag{124b}$$

From equations (46) and (53), with (47) and (43), we notice that the dephasing and decay rates (93) and (94) strongly depend on the i-layer thickness $x_2 - x_0$. In figure 5a, we represent the decay rates $\gamma_\parallel^P, \gamma_\parallel^E, \gamma_\parallel^{EM}$ for the three dissipative couplings, with the phonons of the crystal vibrations, the conduction electrons and holes, and the free electromagnetic field, $\gamma_\parallel = \gamma_\parallel^P + \gamma_\parallel^E + \gamma_\parallel^{EM}$. We also represent the fluctuation rate (95) with the components (48) for the two neighboring conduction regions n and p, $\gamma_n^2 = \left[\gamma_n^{(n)}\right]^2 + \left[\gamma_n^{(p)}\right]^2$. In figure

5b, we represent the coupling coefficients for a longitudinal and a transversal structure. For all these coefficients, we get quasi-exponential variations with the i-layer thickness $x_2 - x_0$. We notice that, in these structures, the phonon decay rate $\gamma_{\|}^{P}$, which is unavoidable, dominates the electric decay rate $\gamma_{\|}^{E}$, which depends on the separation barriers, while the electromagnetic decay rate $\gamma_{\|}^{EM}$ is negligible. It is remarkable that the decay rate of a quantum

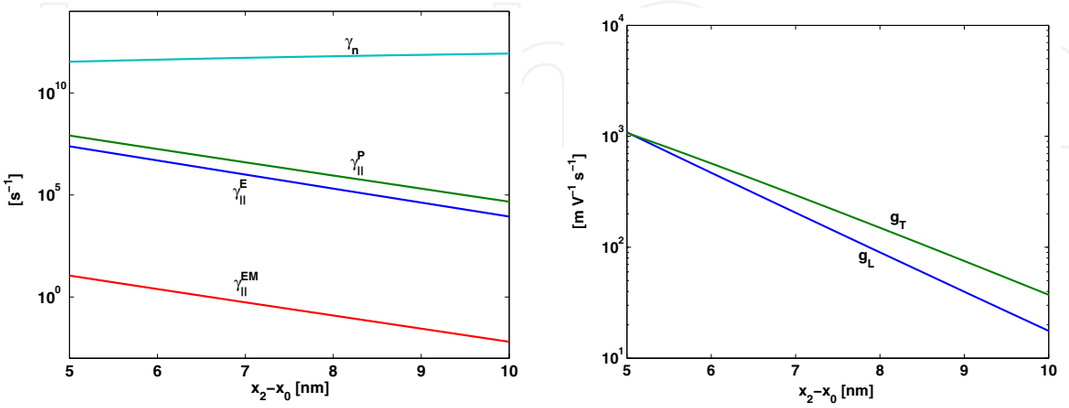

(a) (b)

Fig. 5. (a) The dependence of the dissipative coefficients on the i-zone thickness; (b) The dependence of the coupling coefficients on the i-zone thickness, for a longitudinal and a transversal structure.

injection dot, with a value around $10^7 s^{-1}$, is significantly lower than the decay rates of other $GaAs$ structures, which are at least somewhere around $10^{12} s^{-1}$ (13). From figure 5b, we notice that, although the two coupling coefficients are calculated with completely different dipole moments, g_L with (42b)-(42c), and g_T with (42a), the values of these coefficients are approximately equal for small values of $x_2 - x_0$, and keep near values for thicker i-zones.

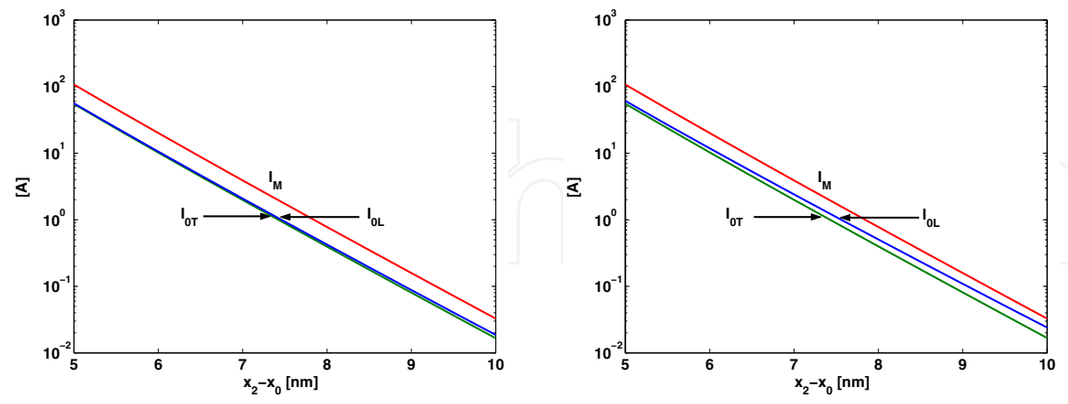

(a) (b)

Fig. 6. The dependence of the threshold currents on the thicknesses of the i-zone for two values of the transmission coefficient of the output mirror: (a) $\mathcal{T} = 0.1$; (b) $\mathcal{T} = 0.5$.

From equations (121), we notice that the dissipative rates $\gamma_{\|}, \gamma_{\perp}$ and the coupling coefficient g_L (g_T), determine the threshold current I_{0L} (I_{0T}). In figure 6a we represent the dependence

of these currents in comparison with the maximum current I_M, for two values of the output transmission coefficient $\mathcal{T}$. We notice that the operation condition $I_{0L}, I_{0T} > I_M$ is satisfied for both values of these coefficients. This property can be understood from the analytical expressions (121) or (124), having in view that the dephasing rate $\gamma_\perp$ and the square of the coupling coefficient g_L (g_T) are proportional to the square of the dipole moment, which means that the operation condition does not depend on this moment. Since the quantum

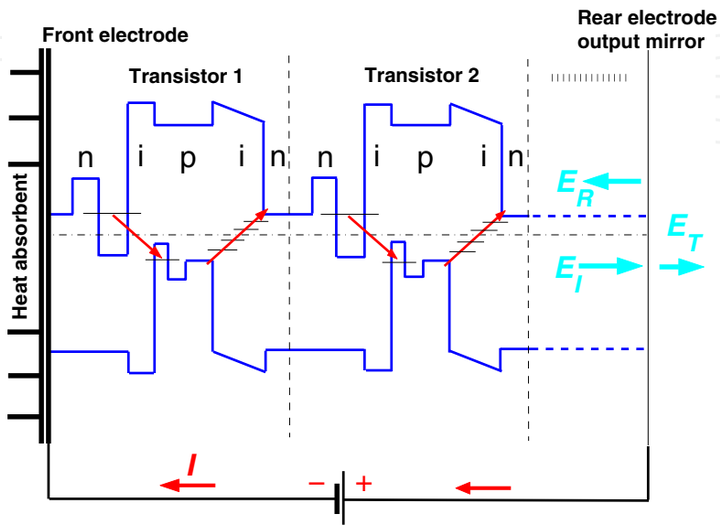

Fig. 7. Quantum heat converter, as a packet of super radiant transistors, thermally coupled to a heat absorbent. While a current I is injected in the device, an electromagnetic flow is obtained, mainly on the account of the heat absorption.

dot density N_e is determined by physical conditions, according to (25), the threshold current (121) can be controlled only by the number of super radiant transistors $\bar{N}_t$ in the structure. In our calculations we considered a number of superadiant transistors $\bar{N}_t = 1045$. While the heat propagates from the heat absorbent (see figure 7) throughout the semiconductor structure, a portion of this heat is absorbed by every super radiant transistor, producing a temperature decrease from the front electrode to the rear one. In figure 8a we represent the electric power and the radiation power as functions of the injected current, for a longitudinal and a transversal configuration of the device. A radiation power arises only when the injection current exceeds a threshold value. From (121a) and (121b), we notice that, due to the factor $\frac{L_D}{A_D^{1/2}}$ in the radiation term of the population inversion, the threshold current of a transversal device is lower than that of a longitudinal one. However, due the same factor at the denominator of (120b), the increase of the radiation power with the injection current is lower for a transversal device than for a longitudinal one. In figure 8b the total temperature variation in the semiconductor structure is represented. We notice that a rather high power of 200 W, that means 0.500 MW from an active area of 1 m^2, can be obtained at a rather low temperature difference of about $7\ ^0C$.

The radiation power of a transversal device becomes much higher by increasing the transmission coefficient from $\mathcal{T} = 0.1$ to $\mathcal{T} = 0.5$ and the transition dipole moment by diminishing the thickness of the i-zone from $x_2 - x_0 = 6.5\ nm$ to $x_2 - x_0 = 6\ nm$ as is represented in figure 9. In this case, the threshold current of the transversal device becomes significantly lower than that of the longitudinal one. The threshold current of the longitudinal

device is sgnificantly lowered by decreasing the transmission coefficient from $\mathcal{T} = 0.5$ to $\mathcal{T} = 0.2$ as is represented in figure 10.

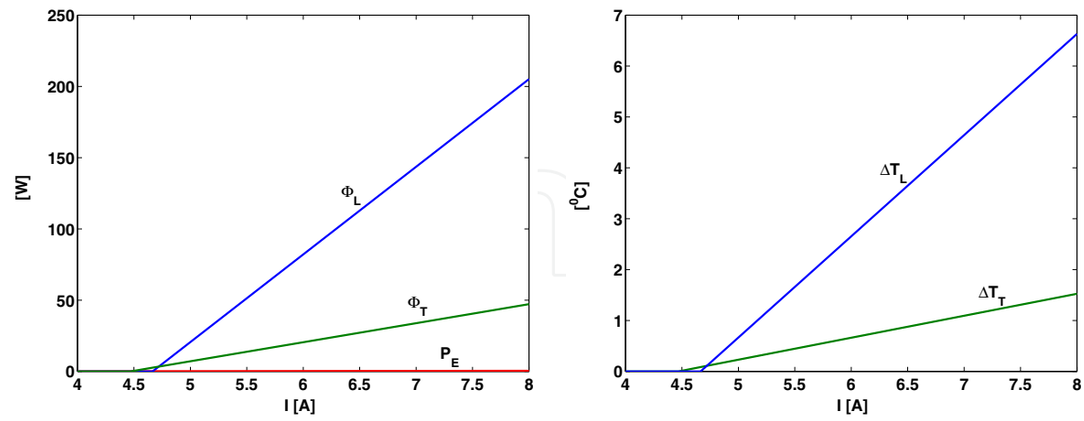

(a) (b)

Fig. 8. (a) The radiation powers Φ_L and Φ_T and the electric power P_E as functions of the injection current I, for $x_2 - x_0 = 6.5\ nm$, $\mathcal{T} = 0.1$, and $\gamma_F = 10^7\ s^{-1}$; (b) The temperature variations $\Delta T_L,\ \Delta T_T$ as functions of the injection current I.

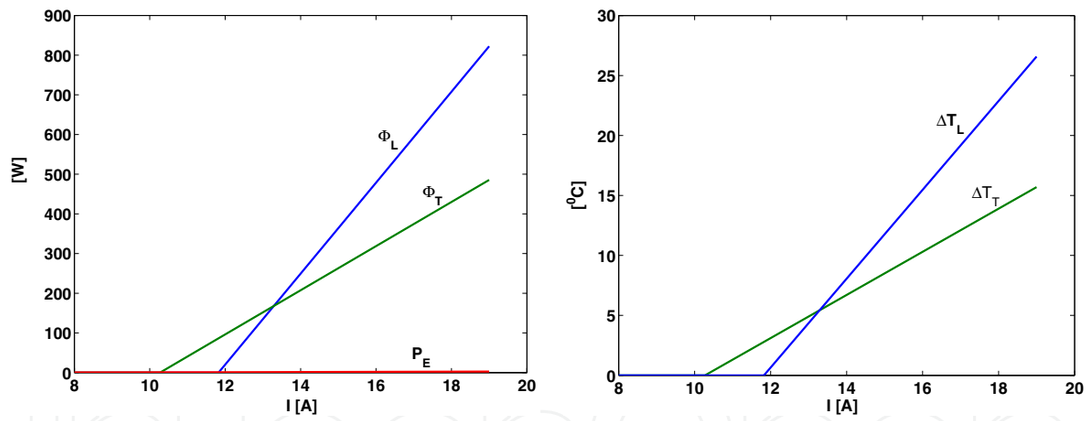

(a) (b)

Fig. 9. The radiation powers Φ_L and Φ_T, the electric power P_E, and the temperature variations $\Delta T_L,\ \Delta T_T$ as functions of the injection current, for $x_2 - x_0 = 6\ nm$, $\mathcal{T} = 0.5$, and $\gamma_F = 10^7\ s^{-1}$.

It is remarkable that in the three cases represented in figures 8-10 the electric power dissipated in the device by the injection current I is much lower than the super radiant power. This is because, as one can notice also from (120), the super radiant power produced by the injected current corresponds to the high transition energy $\hbar\omega_0$ between the two zones n and p, while the power electrically dissipated by this current corresponds to a very low potential difference $U_c - U_{c1}$, necessary for carrying this current through the two rather thin highly conducting zones n and p (figure 7b). The difference between these two powers is obtained by heat absorption, when the electrons are excited from the lower potential of the p-zone to the higher

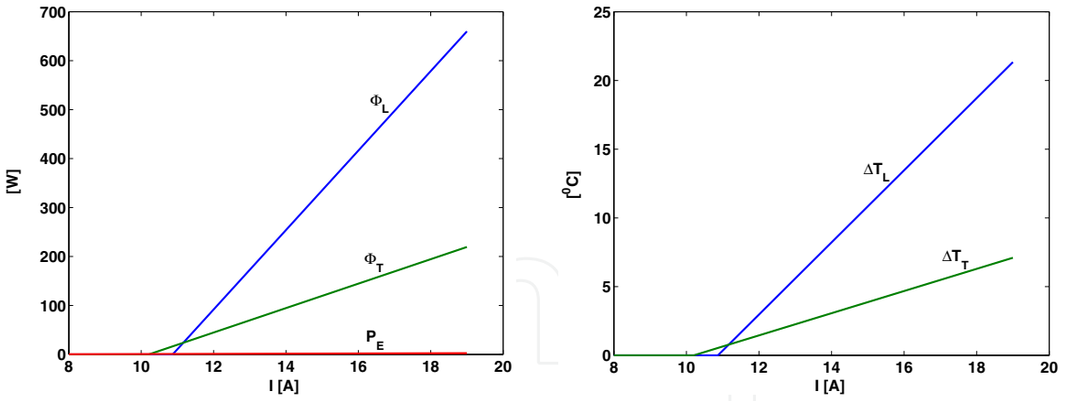

(a) (b)

Fig. 10. The radiation powers Φ_L and Φ_T, the electric power P_E, and the temperature variations ΔT_L, ΔT_T as functions of the injection current, for $x_2 - x_0 = 6\ nm$, $\mathcal{T} = 0.2$, and $\gamma_F = 10^7\ s^{-1}$.

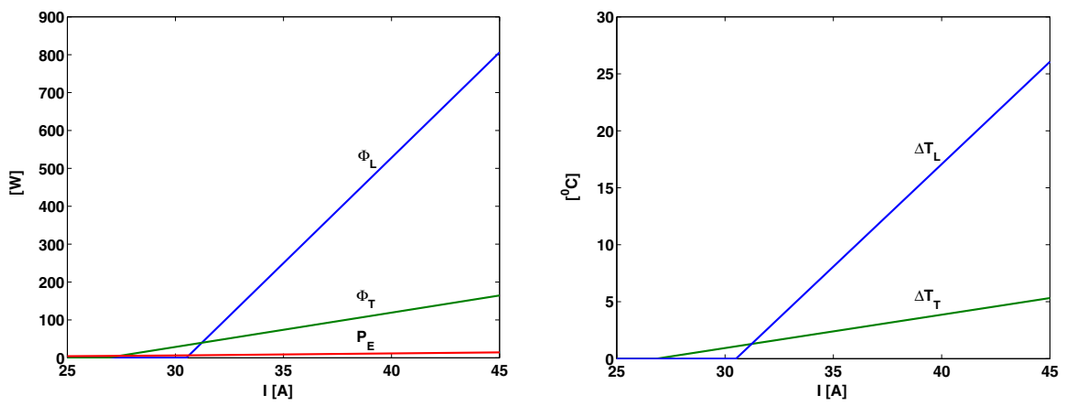

(a) (b)

Fig. 11. The radiation powers Φ_L and Φ_T, the electric power P_E, and the temperature variations ΔT_L, ΔT_T as functions of the injection current, for $x_2 - x_0 = 5.5\ nm$, $\mathcal{T} = 0.5$, and $\gamma_F = 10^8\ s^{-1}$.

potential of the n-zone of the base-collector junction. In figure 11 we consider a much larger decay rate of the electromagnetic field, $\gamma_F = 10^8\ s^{-1}$ instead of $\gamma_F = 10^7\ s^{-1}$, when the operation conditions (124) are also satisfied. In this case, we also obtain a high radiation power, but with a higher injection current, which, however, does not produce an important electrical power P_E, dissipated in the device.

We study the time evolution of a quantum heat converter, by solving the time dependent system of equations (110), for a step current injected at the initial $t = 0$, and a fluctuation that arises at a certain time $t > 0$. Non-Markovian fluctuations are time-evolutions of polarization, population and field due to the self-consistent field of the environment particles that, in our case, are the quasi-free electrons and holes in the conduction regions of the device. In figure 12, we represent the dynamics of a longitudinal device with a thickness of the i-zone $x_2 - x_0 = 5.5\ nm$ and a transmission coefficient of the output mirror $\mathcal{T} = 0.1$, while the threshold current is $I_{0L} = 24.1149\ A$ and the maximum current is $I_M = 46.0995\ A$. We consider a step

current $I = 45\ A$ injected at time $t = 0$. In the Markovian approximation, the super radiant power $\Phi_L(t)$ of a longitudinal quantum heat converter is generated as in figure 12a, while the population $w(t)$ and polarization variables $u(t)$, $v(t)$ have the time-evolutions represented in figure 12b. The sudden jumps of the polarization variables in figure 12b, are detailed in

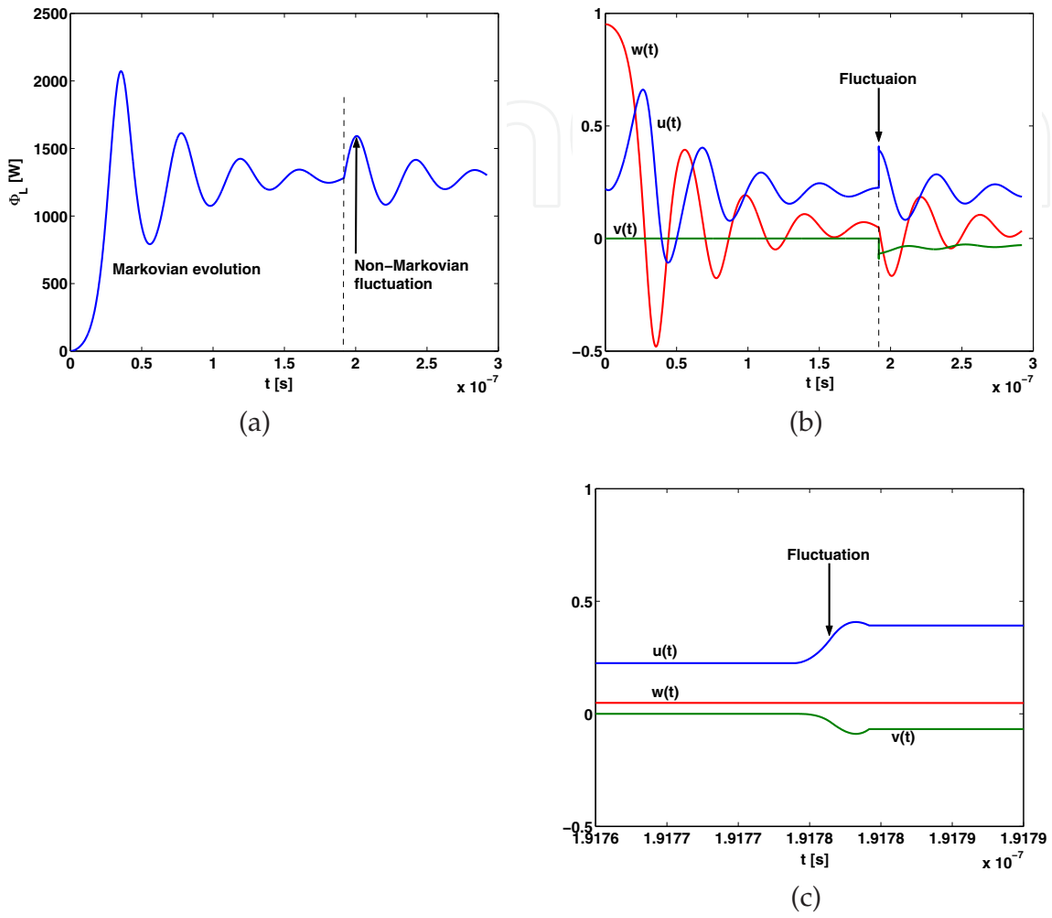

Fig. 12. Dynamics of a longitudinal super radiant device with $x_2 - x_0 = 5.5\ nm$ and $\mathcal{T} = 0.1$ when a step current of $I = 45\ A$ is injected in the device: (a) super radiant power; (b) polarization and population; (c) polarization fluctuation in a short timescale.

figure 12c, in a short timescale. At $t = 0$, the population increases from the equilibrium value w_T for the temperature T, to $w(0) = w_T + 2I/(eN_eA_D\gamma_{\|})$ and, after that, while the radiation field increases, the population decreases tending to an asymptotic value. With an appropriate choice of the phase of the initial polarization, $v(0) = 0$, $u(0)$ takes a value corresponding to the maximum value $-w_T$ of the Bloch vector, which is $u(0) = \sqrt{[w_T^2 - w^2(0)]/(2 - \mathcal{T})}$. In the Markovian approximation, the electromagnetic power is growing to a certain value, and after a short oscillation tends to the asymptotic value that according to (120a) is $\Phi_L = 1.2843 \times 10^3\ W$. However, in the non-Markovian approximation, random fluctuations of the polarization, population, and field arise. These fluctuations are described by the time integrals in the polarization equations (110a) and (110b) depending on the time-dependent phase term $\phi_n(t')$, with a mean-value of the fluctuation time $\tau_n = 1/\gamma_n$. From figure 5a, we notice that the fluctuation rate γ_n is four orders higher than the decay rate $\gamma_{\|}$, corresponding to the timescale

of the Markovian processes. In equations (110a) and (110b), we take a positive fluctuation with a duration tn $\tau_n = 2.6305 \times 10^{-12} s$, followed by a negative one with the same duration. In figure 12c such a fluctuation is represented in a short timescale, specific to the non-Markovian fluctuations, while in figures 12a and 12b it is represented in a long timescale specific to the Markovian processes. We notice that, while the polarization variables $u(t)$ and $v(t)$, which depend on the transition elements of the density matrix, undertake considerable variations in a fluctuation time, for population and super radiant field these variations only initialize long time oscillations.

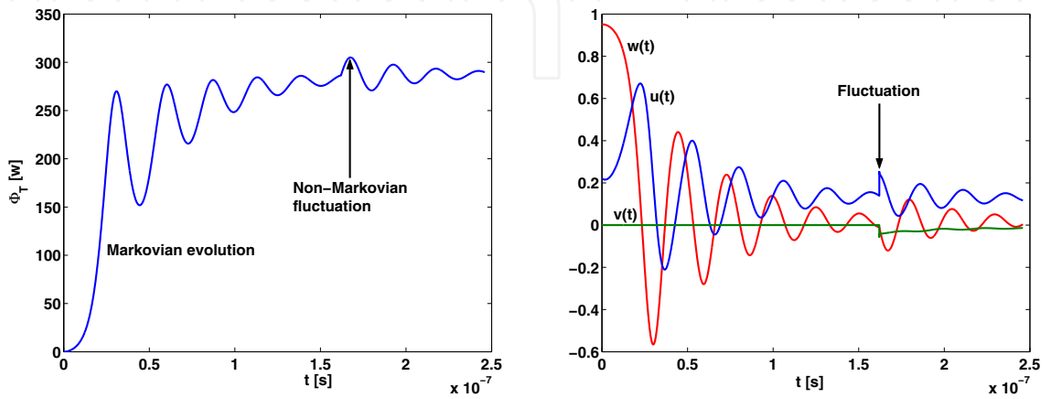

(a) (b)

Fig. 13. Dynamics of a transversal super radiant device with $x_2 - x_0 = 5.5\ nm$ and $\mathcal{T} = 0.1$ when a step current of $I = 45\ A$ is injected: (a) Superradiant power; (b) Population and polarzation.

In figure 13, we represent the dynamics of the transversal device with the same semiconductor structure and injected current, while the threshold current takes a lower value $I_{0T} = 23.4528\ A$. This decrease of the threshold current for a transversal device, in comparison with a longitudinal one with the same semiconductor structure, is obtained due to the field amplification on the longer path of the field propagation in the plane of the quantum dot layers, which is described by the term $c\mathcal{T}\frac{L_D}{A_D^{1/2}}$ in equations (121). However, this small difference is not very significant, since, according to equation (83), a longer propagation path leads also to a higher decay rate of the field, i.e. to an increase of the dissipative term $1_L\gamma_F$. We notice that, while the radiation power is lower, this device is much less sensitive to the thermal fluctuations described by the non-Markovian term. This decrease of the radiation power for a transversal device, in comparison with a longitudinal one with the same semiconductor structure, is obtained due to the factor $\frac{A_D^{1/2}}{L_D}$ at the denominator of equation (120b). An essential advantage of a transversal quantum heat converter, in comparison with a longitudinal one, consists in injection electrodes as zero-transmission mirrors, i.e. these electrodes are thick metalizations, providing an uniform current injection in the device. For an uniform current injection, a longitudinal quantum heat converter needs a special output structure, as a high transmission output Fabry-Perot cavity (4). Although for a transversal device we obtained a lower radiation power than a longitudinal one, it could be advantageous for some applications: for instance to obtain a powerful radiation device, as a stack of many transversal quantum heat converters. Another application could be an electric generator with the three semiconductor devices of the system, transversal quantum heat converter, quantum

injection system, and total quantum injection system, in the same plane, eventually stuck on the same pad.

In figures 12 and 13, we considered a positive fluctuation followed by a negative one, which means an integration over a first interval of time $\tau_n = 1/\gamma_n$ with a phase $\phi_n = 0$ followed by an integration over a second interval of time τ_n with a phase $\phi_n = \pi$ in the polarization equations (110a) and (110b).

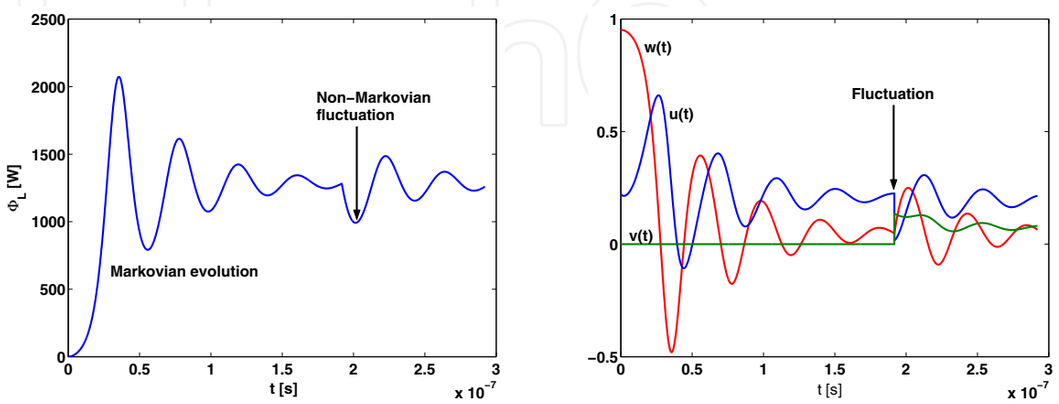

(a) (b)

Fig. 14. Dynamics of a longitudinal super radiant device with a negative fluctuation ($\phi_n = \pi$), followed by a positive one ($\phi_n = 0$).

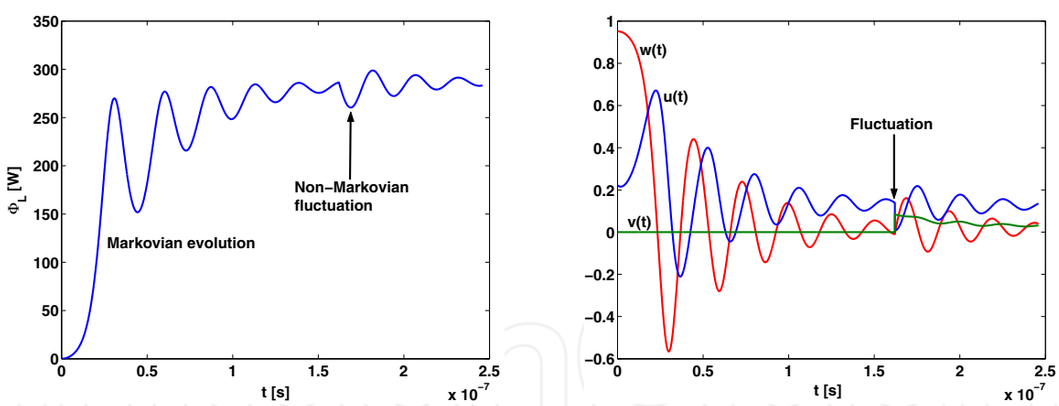

(a) (b)

Fig. 15. Dynamics of a transversal super radiant device with a negative fluctuation ($\phi_n = \pi$), followed by a positive one ($\phi_n = 0$).

Changing the phases of the fluctuations, i.e. taking a negative fluctuation followed by a positive one (figures 14 and 15), we get similar evolutions but with opposite signs. Obviously, the realistic evolution of a device is the result of the random phases ϕ_n, arising during the whole evolution of the system. Thus, the system dynamics takes a noisy form, with the polarization undertaking rapid variations during a fluctuation time, while the population and the super radiant field are only initialized into slow oscillations.

7. Conclusions

We presented a new kind of quantum dots, with a quantum well for electrons in the n-region of an n-i-p heterostructure, and a quantum well for holes in the p-region of this structure. These quantum wells are separated from the two n and p conduction regions by transparent potential barriers, and separated from one another by the potential barrier of the i-region. Such a quantum dot, we call "quantum injection dot", can be compared with a conventional quantum dot, as a small semiconductor region with a narrower forbidden band in a much larger i-region of an n-i-p semiconductor structure. Quantum injection dots have mainly been conceived for conversion of environmental heat into usable energy, while the conventional quantum dots are mainly used in information technology. A quantum injection dot differs in many respects from a conventional quantum dot, where the quantum well for holes is placed under the quantum well for electrons, as conduction and valence bands of the same semiconductor region: (1) while a quantum injection dot is supplied with electrons and holes from the two conduction regions by quantum tunneling through the n and p separation barriers, without any energy increase, a conventional quantum dot is supplied with electrons and holes only by providing a substantial energy, necessary to raise these electrons and holes from the n and p conduction regions to the conduction and valence bands of the i-region, from where they fall in the two potential wells of the quantum dot; (2) a quantum injection dot provides the electron transfer from the n-region to the p-region only by quantum transitions, while the electron transfer provided by a conventional quantum dot includes additional transport processes from the two n and p regions to the i-region where this quantum dot is located; (3) a quantum injection dot is a one-electron normalized two-level quantum system, while a conventional quantum dot is a confinement semiconductor region where many electrons and holes are simultaneously present to provide a larger probability for the super radiant transitions. In comparison with a conventional quantum dot, a quantum injection dot is much less dissipative, and, due to its simpler structure, enables a much higher packing degree in a semiconductor structure.

We studied a system of quantum injection dots by using the available means of quantum mechanics: (1) we calculated wave-functions, dipole moments, and eigenvalue equation for energy; (2) we derived equations for the dissipative super radiant dynamics of the system; (3) we obtained analytical coefficients depending only on physical characteristics and universal constants, without any phenomenological parameter. In the dynamics of a quantum dot system, we distinguish five dissipative processes: (1) correlated transitions with phonons of the crystal lattice vibrations, which is the dominant dissipation process (2) correlated transitions with quasi-free electrons and holes in the conduction regions, (3) correlated transitions with the quasi-free electromagnetic field, which are negligible, (4) transitions stimulated by the thermal fluctuations of the self-consistent field of the electrons and holes in the conduction regions, (5) non-Markovian processes induced by these fluctuations. However, we found that the fluctuation time is much shorter than the decay time, which means that the system is in fact quasi-Markovian, while the non-Markovian fluctuations manifest themselves only as a noise. For the propagation of the electromagnetic field throughout the semiconductor structure, by taking into account the dissipative interaction with the quasi-free electrons an holes in the conduction regions, we obtained an analytical expression of the field decay rate as a function of effective masses, frequency, and propagation path.

We studied a device converting environmental heat into coherent electromagnetic energy in two versions: (1) longitudinal quantum heat converter, with the electromagnetic field propagating in the direction of injected current, i.e. emerging from the surface

the semiconductor structure, and (2) transversal quantum heat converter, with the electromagnetic field propagating in a perpendicular direction to the injected current, i.e. emerging from a lateral surface of the semiconductor structure. We found operation conditions for the physical characteristics of the semiconductor structure. We studied the dependence of the dissipative rates, coupling coefficients, and threshold currents as functions of the i-region thickness, which enables the control of these quantities in a large field of values. We found that the operation conditions do not depend on the i-layer thickness. When this thickness is decreased, the injected current and the corresponding super radiant power increase. However, these quantities of interest can not be indefinitely increased, especially due to the temperature variation induced by the heat propagation throughout the structure, which tends to produce an atomic detuning of the quantum dot layers. We highlighted the super radiant dissipative dynamics under a step current injection, and thermal fluctuations of the conduction electrons and holes.

8. References

[1] Kent D. Choquette and John F. Klem, Long wavelength vertical cavity surface emitting laser, US 6,931,042 B2 (US Patent Office, Aug. 16, 2005).
[2] Ashkan A. Arianpour, James P. McCanna, Joshua R. Windmiller, Semeon Y. Litvin, Photovoltaic device employing a resonator cavity, US 2008/0128023 A1 (US Patent Office, Jun. 05, 2008).
[3] E. Stefanescu, Master equation and conversion of environmental heat into coherent electromagnetic energy, Prog. Quantum Electron. 34 (2010) 349-408.
[4] Eliade Stefanescu, Lucien Eugene Cornescu, Longitudinal quantum heat converter, US 20090007950 (US Patent Office, 01-08-2009), http://www.freepatentsonline.com/y2009/0007950.html.
[5] Eliade Stefanescu, Lucien Eugene Cornescu, Transversal quantum heat converter, US 20100019618 (US Patent Office, 01-28-2010), http://www.freepatentsonline.com/y2010/0019618.html.
[6] Eliade Stefanescu, Lucien Eugene Cornescu, Quantum injection system, US 20090007951 (US Patent Office, 01-08-2009), http://www.freepatentsonline.com/y2009/0007951.html.
[7] E. Stefanescu, W. Scheid, and A. Sandulescu, Non-Markovian master equation for a system of Fermions interacting with an electromagnetic field, Ann. Phys. 323 (2008) 1168-1190.
[8] T. Fließbach, Statistische Physik, Lehrbuch zur Theoretischen Physik IV (Elsevier, München 2007).
[9] G. W. Ford, J. T. Lewis, and R. F. O'Connell, Master Equation for an Oscillator Coupled to the Electromagnetic Field, Ann. Phys. 252 (1996) 362-385.
[10] V. M. Axt and S. Mukamel, Nonlinear Optics of semiconductor and moleclar nanostructures, Rev.Mod..Phys. 70 (1998) 145-287.
[11] Eliade Stefanescu, Dynamics of a Fermi system with resonant dissipation and dynamical detailed balance, Physica A 350 (2005) 227-244.
[12] Haward Carmichael, an Open Quantum System Approach to Quantum Optics, in Lecture notes in Physics (Springer Verlag, Berlin 1993).
[13] Hartmut Haug and Antti-Pekka Jauho, Quantum Kinetics in Transport and Optics of Semiconductors (Springer-Verlag, Berlin, Heidelberg, New York, 1998).
[14] Günter Mahler and Volker A. Weberruß, Quantum Networks - Dynamics of Open Nanostructures (Springer-Verlag, Berlin, Heidelberg, New York, 1995).

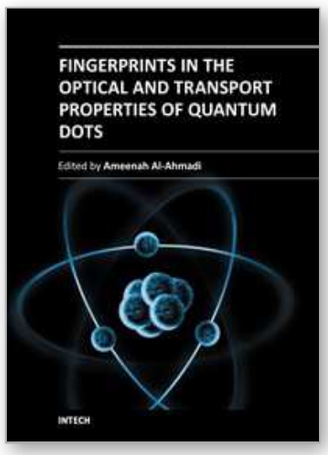

Fingerprints in the Optical and Transport Properties of Quantum Dots

Edited by Dr. Ameenah Al-Ahmadi

ISBN 978-953-51-0648-7
Hard cover, 468 pages
Publisher InTech
Published online 13, June, 2012
Published in print edition June, 2012

The book "Fingerprints in the optical and transport properties of quantum dots" provides novel and efficient methods for the calculation and investigating of the optical and transport properties of quantum dot systems. This book is divided into two sections. In section 1 includes ten chapters where novel optical properties are discussed. In section 2 involve eight chapters that investigate and model the most important effects of transport and electronics properties of quantum dot systems This is a collaborative book sharing and providing fundamental research such as the one conducted in Physics, Chemistry, Material Science, with a base text that could serve as a reference in research by presenting up-to-date research work on the field of quantum dot systems.

How to reference

In order to correctly reference this scholarly work, feel free to copy and paste the following:

Eliade Stefanescu (2012). Quantum Injection Dots, Fingerprints in the Optical and Transport Properties of Quantum Dots, Dr. Ameenah Al-Ahmadi (Ed.), ISBN: 978-953-51-0648-7, InTech, Available from: http://www.intechopen.com/books/fingerprints-in-the-optical-and-transport-properties-of-quantum-dots/quantum-injection-dots

INTECH
open science | open minds

InTech Europe
University Campus STeP Ri
Slavka Krautzeka 83/A
51000 Rijeka, Croatia
Phone: +385 (51) 770 447
Fax: +385 (51) 686 166
www.intechopen.com

InTech China
Unit 405, Office Block, Hotel Equatorial Shanghai
No.65, Yan An Road (West), Shanghai, 200040, China
中国上海市延安西路65号上海国际贵都大饭店办公楼405单元
Phone: +86-21-62489820
Fax: +86-21-62489821

IntechOpen